

AN INVESTIGATION OF TWO-PHASE FLOWS
WITH EVAPORATION

A THESIS

Presented to

The Faculty of the Division of Graduate
Studies and Research

By

Douglass Stephen Lubbers

In Partial Fulfillment

of the Requirements for the Degree
Master of Science in Mechanical Engineering

Georgia Institute of Technology

June, 1974

ACKNOWLEDGMENTS

It is with a deep sense of gratitude that the author thanks his thesis advisor, Dr. Novak Zuber, for his guidance and encouragement. It was through Dr. Zuber that the author was introduced to the problem and was given much of the academic background required for this study.

The author is indebted to Dr. H. C. Ward and Dr. W. Wulff for serving as members of the reading committee. Their criticisms and suggestions were helpful in the course of reviewing this work.

Special thanks are due the School of Mechanical Engineering and the National Science Foundation (Grant No. GK-16023) for providing financial support during the past year. In addition, the author wishes to express his thanks to those members of the School who preceded him, and who were responsible for the design and construction of the Freon Loop on which the experimental data necessary for this study were gathered.

Finally, the author wishes to express his appreciation to his wife, Susan, for her continued love, devotion, and encouragement. Her assistance during the past year greatly facilitated the completion of the present work.

TABLE OF CONTENTS

	Page
ACKNOWLEDGMENTS.	ii
LIST OF TABLES	v
LIST OF ILLUSTRATIONS.	vii
NOMENCLATURE	ix
SUMMARY.	xii
Part I. EXPERIMENTAL PRESSURE DROP IN EVAPORATIVE TWO-PHASE FLOW.	1
Chapter	
I. INTRODUCTION.	2
1.1 Significance of the Problem	
1.2 Description of Predictive Methods	
1.2.1 Homogeneous Model	
1.2.2 Separated Flow Model	
1.2.3 Mixture Model	
1.3 Purpose	
II. EXPERIMENTAL PROGRAM.	14
2.1 Method of Experiments	
2.2 Accuracy of Data	
III. RESULTS AND DISCUSSION.	17
IV. CONCLUSIONS	28
Part II. A CONSTITUTIVE EQUATION FOR THE NET RATE OF VAPOR GENERATION IN SUBCOOLED BOILING.	29
I. INTRODUCTION.	30
1.1 Significance of the Problem	
1.2 Purpose	

Chapter	Page
II. PRESENT STATE OF THE ART.	32
2.1 Characteristics of Thermal Equilibrium Flow	
2.2 Characteristics of Thermal Non-Equilibrium Flow	
2.2.1 Superheated Liquid Only	
2.2.2 Bubbly Flow--Superheated Liquid with Vapor Bubbles	
2.2.3 Bubbly Flow--Subcooled Liquid with Vapor Bubbles	
2.3 Formal Approach	
2.4 Approximation Methods	
2.5 Conclusions	
III. FORMULATION	43
3.1 Model	
3.2 Decoupling of the System	
3.3 Mixture Density and True Vapor Quality	
IV. COMPARISON WITH EXPERIMENTS AND DISCUSSION.	57
V. CONCLUSIONS	62
Appendix	
A. DESCRIPTION OF PREDICTIVE TECHNIQUES.	64
B. RESULTS OF PREDICTIVE METHODS AND EXPERIMENTAL DATA.	81
BIBLIOGRAPHY	110

LIST OF TABLES

Table		Page
1.	Results of Predictive Methods and Experimental Data. System Pressure = 150 psia.	82
2.	Results of Predictive Methods and Experimental Data. System Pressure = 150 psia.	83
3.	Results of Predictive Methods and Experimental Data. System Pressure = 150 psia.	84
4.	Results of Predictive Methods and Experimental Data. System Pressure = 150 psia.	85
5.	Results of Predictive Methods and Experimental Data. System Pressure = 150 psia.	86
6.	Results of Predictive Methods and Experimental Data. System Pressure = 175 psia.	87
7.	Results of Predictive Methods and Experimental Data. System Pressure = 175 psia.	88
8.	Results of Predictive Methods and Experimental Data. System Pressure = 175 psia.	89
9.	Results of Predictive Methods and Experimental Data. System Pressure = 175 psia.	90
10.	Results of Predictive Methods and Experimental Data. System Pressure = 175 psia.	91
11.	Results of Predictive Methods and Experimental Data. System Pressure = 175 psia.	92
12.	Results of Predictive Methods and Experimental Data. System Pressure = 175 psia.	93
13.	Results of Predictive Methods and Experimental Data. System Pressure = 175 psia.	94
14.	Results of Predictive Methods and Experimental Data. System Pressure = 175 psia.	95

Table	Page
15. Results of Predictive Methods and Experimental Data. System Pressure = 175 psia.	96
16. Results of Predictive Methods and Experimental Data. System Pressure = 175 psia.	97
17. Results of Predictive Methods and Experimental Data. System Pressure = 175 psia.	98
18. Results of Predictive Methods and Experimental Data. System Pressure = 175 psia.	99
19. Results of Predictive Methods and Experimental Data. System Pressure = 175 psia.	100
20. Results of Predictive Methods and Experimental Data. System Pressure = 195 psia.	101
21. Results of Predictive Methods and Experimental Data. System Pressure = 195 psia.	102
22. Results of Predictive Methods and Experimental Data. System Pressure = 195 psia.	103
23. Results of Predictive Methods and Experimental Data. System Pressure = 195 psia.	104
24. Results of Predictive Methods and Experimental Data. System Pressure = 195 psia.	105
25. Results of Predictive Methods and Experimental Data. System Pressure = 195 psia.	106
26. Results of Predictive Methods and Experimental Data. System Pressure = 195 psia.	107
27. Results of Predictive Methods and Experimental Data. System Pressure = 195 psia.	108
28. Results of Predictive Methods and Experimental Data. System Pressure = 195 psia.	109

LIST OF ILLUSTRATIONS

Figure	Page
1. Non-Dimensional Viscosity Ratio versus Quality for $\mu_f/\mu_g = 6.68$	7
2. Pressure Drop Estimation in Two-Phase Flow with Evaporation $P_s = 150$ psia $R_{ei} = 63780$	18
3. Pressure Drop Estimation in Two-Phase Flow with Evaporation $P_s = 175$ psia $R_{ei} = 67740$	19
4. Pressure Drop Estimation in Two-Phase Flow with Evaporation $P_s = 175$ psia $R_{ei} = 115606$	20
5. Pressure Drop Estimation in Two-Phase Flow with Evaporation $P_s = 195$ psia $R_{ei} = 60220$	21
6. Pressure Drop Estimation in Two-Phase Flow with Evaporation $P_s = 195$ psia $R_{ei} = 62675-65264$	22
7. Pressure Drop Estimation in Two-Phase Flow with Evaporation $P_s = 195$ psia $R_{ei} = 30121$	23
8. Increase of Experimental Pressure Drop with Onset of Nucleation (Chart Divisions) $P_s = 175$ psia $R_{ei} = 115606$	24
9. Increase of Experimental Pressure Drop with Onset of Nucleation (Actual psi) $P_s = 175$ psia $R_{ei} = 115606$	25
10. Experimental Repeatability.	27
11. Comparison Between Predicted and Measured Vapor Void Fraction. Data of Martin.	60
12. Comparison Between Predicted and Measured Vapor Void Fraction. Data of Lobachev, et al.	60
13. Comparison Between Predicted and Measured Vapor Void Fraction. Data of Staub, et al.	61

Figure	Page
14. Ratio of Two-Phase Pressure Gradient to Pressure Gradient for 100 Per Cent Liquid Flow as a Function of Quality and Pressure, Steam-Water (Martinelli-Nelson).	66
15. Ratio $(\Delta p_{\text{fric}})_{\text{TP}}/(\Delta p)_{\text{fo}}$ as a Function of Exit Quality and Pressure, Steam-Water (Martinelli-Nelson).	67
16. Void Fraction, α , as a Function of Quality and Absolute Pressure, Steam-Water (Martinelli-Nelson).	69
17. Multiplier, r_2 , as a Function of Pressure for Various Exit Qualities, Steam-Water (Martinelli-Nelson).	70
18. Effect of Mass Velocity on the Value of ϕ_{fo}^2 at a Pressure of 68.9 bar.	72
19. Two-Phase Friction Pressure Drop Correlation (Baroczy).	73
20. Mass Velocity Correction versus Property Index (Baroczy).	74

NOMENCLATURE

A	cross sectional area
a	thermal diffusivity
c_p	specific heat at constant pressure
C_o	distribution parameter
D_h	hydraulic diameter of the cross section
f	Moody friction factor
G	fluid mass flux
g	acceleration due to gravity
i	fluid enthalpy
Δi_{fg}	latent heat of vaporization
$J(z')$	rate of bubble nucleation per unit area at z'
k	thermal conductivity
L	length of test section
Δl	difference in length between the non-equilibrium point of net vapor generation and the same point as predicted by equilibrium theory
$m(z, z')$	mass of bubble at z that nucleated at z'
N_s	dimensionless Subcooling number
p	absolute pressure
Δp	pressure drop
Pe	dimensionless Peclet number
$\frac{dp}{dz}$	pressure gradient
Q	volumetric flow rate
\dot{q}_w''	wall heat flux

R_e	dimensionless Reynolds number
t	time, independent variable
T	temperature
ΔT	temperature difference
v	velocity
\bar{V}_{gj}	weighted mean drift velocity for upward bubbly churn flow
x	vapor mass quality
W	mass flow rate
z	axial coordinate
Greek	
α	vapor void fraction
Γ_{eq}	net rate of vapor generation per unit volume, equilibrium model
Γ_g	net rate of vapor generation per unit volume, non-equilibrium model
θ	inclination of test section with respect to horizontal
λ	axial coordinate at point of net vapor generation
μ	fluid absolute viscosity
ξ	wetted perimeter of cross section
ρ	fluid density
$\Delta\rho$	difference between liquid density and vapor density
σ	fluid surface tension
τ	stress tensor
ϕ_f^2	ratio of two-phase pressure gradient to that which would occur if the liquid phase were to flow alone in the duct

ϕ_{fo}^2 ratio of two-phase pressure gradient to that which would occur if the total mass flow rate were to flow as liquid

ϕ_{tt} Lockhart-Martinelli parameter

X_{tt} Lockhart-Martinelli parameter

Ω Baroczy parameter

Ω_{eq} equilibrium frequency of evaporation

Subscripts

accel acceleration component

c value at critical point

d diffusion component

e value at exit of test section

eq value according to equilibrium theory

f liquid

fric frictional component

fo total mass flow rate as liquid

g vapor

grav gravitational component

i value at inlet

m mixture

sat saturation value

sub liquid phase subcooling at point of net vapor generation

total total value

TP two-phase value

Superscript

+ dimensionless quantity

SUMMARY

The present investigation consists of two parts, one experimental, the other analytical.

The experimental program (Part I) is concerned with pressure drop prediction in evaporative two-phase flow systems. In this program, various pressure drop models which are reported in the literature are evaluated against experimental data. The results of the evaluation indicate that present models are inaccurate and inconsistent when applied to the data obtained from present experiments. In addition, the experimental data show an increase of the pressure gradient in the region of two-phase flow.

As is shown in the experimental program, accurate prediction of pressure drop is incumbent upon correct estimation of vapor void fraction. The analytical program (Part II) is concerned with the development of a constitutive equation of net vapor generation in subcooled boiling two-phase flows. It is developed from a model which is applicable to steady-state as well as transient flows.

The analysis yields expressions for the true mixture density and the true vapor quality in thermal non-equilibrium conditions, that is, for steady-state or transient subcooled boiling. A comparison of predicted values with available experimental data shows good agreement.

Part I
EXPERIMENTAL PRESSURE DROP IN
EVAPORATIVE TWO-PHASE FLOW

CHAPTER I

INTRODUCTION

1.1 Significance of the Problem

The occurrence of two phase, single or two-component flows in pipelines is characteristic of many processes in modern petroleum, chemical, and nuclear systems. Problems associated with such flows include the inability to predict with accuracy the pressure losses and void fraction in these pipelines. This is particularly true for mixtures in thermodynamic non-equilibrium.

Attempts to predict these quantities to date have mainly focused on the collection of wide ranging experimental data and the correlation of these data to system parameters. Predictions of pressure losses and void fraction for systems other than those used in obtaining these correlations are questionable since it might be expected that the usefulness of the correlations is subject to the limitations of their own data. There have been numerous such correlations, some of which have been widely used. The subject of Part I of the present thesis is to evaluate the results predicted by the various pressure drop models reported in the literature against new experimental data.

1.2 Description of Predictive Methods

A review of the literature indicates that there is no reliable method for predicting pressure loss and void fraction in evaporative two-phase flow systems. Several methods, however, have gained widespread acceptance for design purposes. Models which are evaluated against experimental pressure drops are described below. A review of correlations which are based upon these models is given in Appendix A.

1.2.1 Homogeneous Model

One commonly used approach is to treat the two fluids as if they were one homogeneous mixture with appropriately defined mixture properties (i.e., mixture viscosity and mixture density). The model is based upon the following assumptions:

- i) equal velocities of the vapor and liquid
- ii) thermodynamic equilibrium between the two phases
- iii) the use of a suitably defined single phase friction factor for two-phase flow.

These assumptions imply that the homogeneous model might be expected to yield favorable results for a fog or spray flow pattern occurring at high void fraction. However, it is often applied indiscriminately to problems in which other flow patterns, such as annular flow, would be expected.

Specific volume of a homogeneous mixture is defined [17,20] as the total volumetric flow rate divided by the total mass flow rate

$$\frac{1}{\rho_m} = \frac{Q}{W} = \frac{1-x_{eq}}{\rho_f} + \frac{x_{eq}}{\rho_g} \quad (1.1)$$

where the equilibrium mass quality is defined as

$$x_{eq} = \frac{i(z) - i_{f,sat}}{\Delta i_{fg}} \quad (1.2)$$

and where ρ_f and ρ_g are the densities of the saturated liquid and vapor respectively. Substitution of the above into the basic momentum equation for steady, one-dimensional, homogeneous equilibrium flow in a duct yields [4,20,21]

$$-\left(\frac{dp}{dz}\right)_{total} = \frac{\frac{f_{TP} G^2}{2\rho_f D_h} [1+x_{eq}(\frac{\rho_f}{\rho_g}-1)] + \frac{G^2}{\rho_f} (\frac{\rho_f}{\rho_g}-1) \frac{dx_{eq}}{dz} + \frac{g\rho_f \sin\theta}{[1+x_{eq}(\frac{\rho_f}{\rho_g}-1)]}}{1 - x_{eq} \frac{G^2}{\rho_g} \frac{d\rho_g}{dp}} \quad (1.3)$$

Equation (1.3) is often simplified with the assumption that the fluid densities ρ_f and ρ_g remain constant at their inlet saturation values. This is justified in the literature by reasoning that for the case where pressure drop is small compared to system pressure, the values of ρ_f and ρ_g change very little. The assumption also results in a value of the

denominator for (1.3) of unity. Hence, the simplified form of (1.3) is

$$-\left(\frac{dp}{dz}\right)_{\text{total}} = \frac{f_{TP} G^2}{2\rho_f D_h} [1 + x_{\text{eq}} \left(\frac{\rho_f}{\rho_g} - 1\right)] + \frac{G^2 \left(\frac{\rho_f}{\rho_g} - 1\right) \frac{dx_{\text{eq}}}{dz}}{[1 + x_{\text{eq}} \left(\frac{\rho_f}{\rho_g} - 1\right)]} + \frac{g \rho_f \sin\theta}{[1 + x_{\text{eq}} \left(\frac{\rho_f}{\rho_g} - 1\right)]} \quad (1.3a)$$

The result of this assumption is that the momentum equation (1.3a) may be decoupled from the energy equation for solution.

Term by term integration of this simplified form (1.3a) from the point in the channel where evaporation begins ($z = 0, x_{\text{eq}} = 0$) to some channel location, z , where the equilibrium mass quality is x_{eq} yields

$$-(\Delta p)_{\text{fric}} = \frac{f_{TP} G^2 z}{2\rho_f D_h} \left[1 + \frac{x_{\text{eq}}}{2} \left(\frac{\rho_f}{\rho_g} - 1\right)\right] \quad (1.4)$$

$$-(\Delta p)_{\text{accel}} = G^2 \left(\frac{1}{\rho_g} - \frac{1}{\rho_f}\right) x_{\text{eq}} \quad (1.5)$$

$$-(\Delta p)_{\text{grav}} = \frac{g \sin\theta z}{\left(\frac{1}{\rho_g} - \frac{1}{\rho_f}\right) x_{\text{eq}}} \ln[1 + x_{\text{eq}} \left(\frac{\rho_f}{\rho_g} - 1\right)] \quad (1.6)$$

All the terms in equations (1.4) through (1.6) are known except for the two-phase friction factor, f_{TP} . Most investigators have chosen to attempt a friction factor correlation similar to that obtained in single-phase flow (in terms of the Moody friction factor and the fluid Reynolds number), by specifying artificial definitions of the homogeneous viscosity to use in the definition of the Reynolds number

$$Re = \frac{GD_h}{\mu_m}$$

Numerous definitions are found in the literature of which the most popular are

$$(1) \quad \mu_m = \mu_f, \text{ (Owens [17], 1962)}$$

$$(2) \quad \frac{1}{\mu_m} = \frac{1-x}{\mu_f} + \frac{x}{\mu_g}, \text{ (Isbin et al. [8], 1957 and McAdams et al. [16])}$$

$$(3) \quad \mu_m = (1-x)\mu_f + x\mu_g, \text{ (Cicchitti et al. [5], 1960)}$$

$$(4) \quad \mu_m = \mu_f^{(1-x)} \mu_g^x, \text{ (Hagendorn [7], 1965)}$$

These expressions for mixture viscosity are plotted versus mass quality in Figure 1 to highlight the large differences one could encounter during any analysis involving the definition of viscosity. It can be seen from Figure 1 that

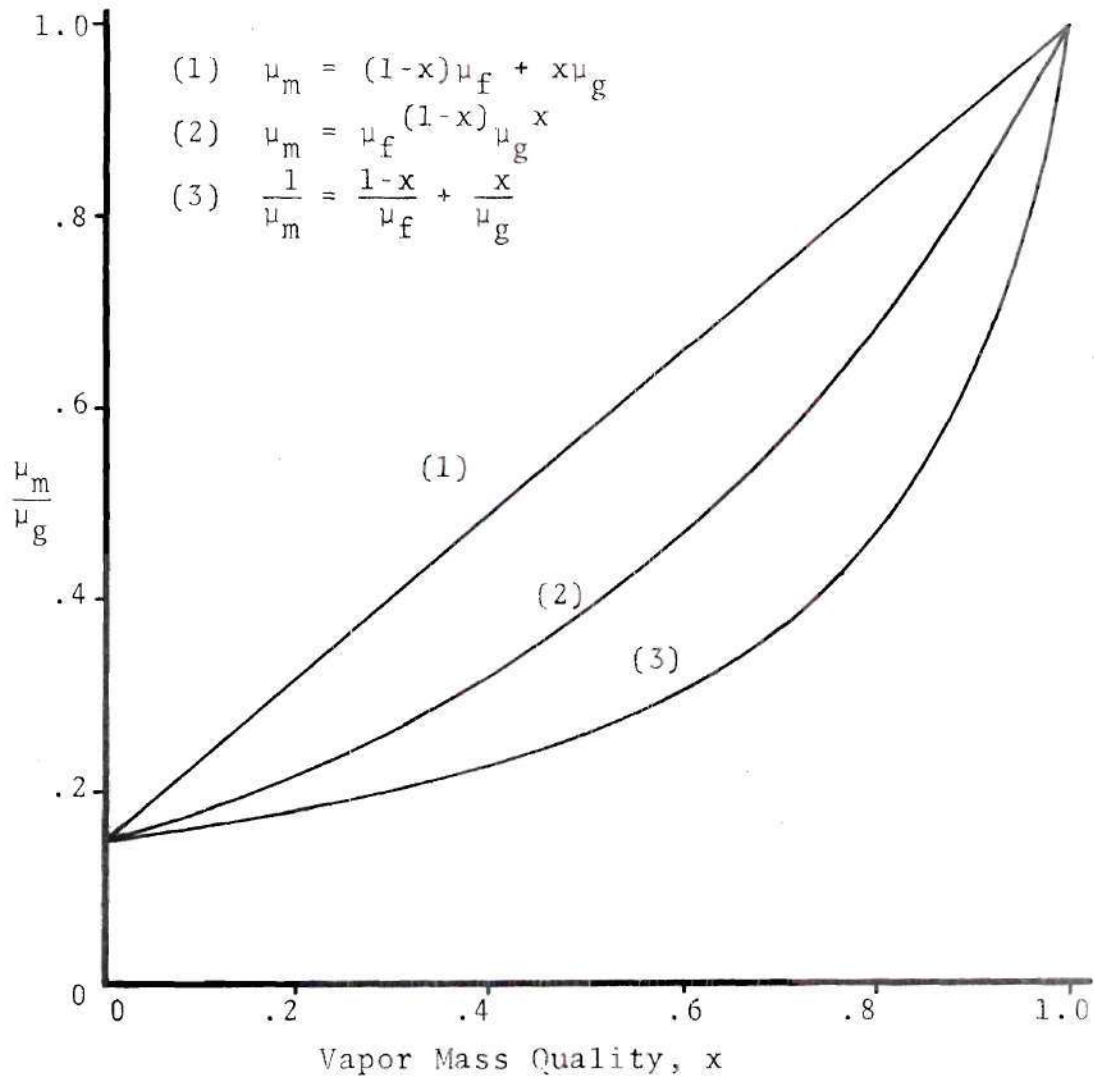


Figure 1. Non-Dimensional Viscosity Ratio Versus Quality for $(\mu_g/\mu_f)_{\text{sat}} = 6.68$

the values can differ by a factor of 2.5 in the worst case. However, one reason for the lack of incentive, so far, to establish an accepted definition is that the dependence of friction factor on viscosity is small for turbulent flow (see Tables 1-28).

1.2.2 Separated Flow Model

An alternative model is one which artificially segregates the phases into two streams. This model may approach physical reality for certain flows (e.g. annular flow) just as the homogeneous model does for fog flow. Assumptions upon which the separated flow model is based are

- i) constant but not necessarily equal velocities for the vapor and liquid phases.
- ii) thermodynamic equilibrium between the phases.
- iii) the use of empirical correlations or simplified concepts to relate the two-phase friction multiplier, ϕ^2 , and the void fraction, α , to the independent variables of the flow.

The basic momentum equation for steady, separated flow may be rearranged to give [4]

$$-\left(\frac{dp}{dz}\right)_{\text{total}} =$$

$$\frac{f_{fo} G^2}{2\rho_f D_h} \phi_{fo}^2 + G^2 \frac{dx_{eq}}{dz} \left[\left\{ \frac{2x_{eq}}{\rho_g \alpha} - \frac{2(1-x_{eq})}{\rho_f (1-\alpha)} \right\} + \frac{d\alpha}{dx_{eq}} \left\{ \frac{(1-x_{eq})^2}{\rho_f (1-\alpha)^2} - \frac{x_{eq}^2}{\rho_f \alpha^2} \right\} \right] +$$

$$\frac{+ g \sin\theta [\rho_g \alpha + \rho_f (1-\alpha)]}{1 + G^2 \left[\frac{d\alpha}{dp} \left\{ \frac{(1-x_{eq})^2}{\rho_f (1-\alpha)^2} - \frac{x_{eq}^2}{\rho_g \alpha^2} \right\} - \frac{x_{eq}^2}{\alpha \rho_g} \frac{d\rho_g}{dp} \right]} \quad (1.7)$$

As for homogeneous flow, the compressibility of the vapor phase may usually be neglected (in which case the denominator is unity), and if it is further assumed that the densities ρ_f and ρ_g , along with the friction factor, f_{fo} , remain constant over the length considered, then term by term integration of the above equation yields

$$-(\Delta p)_{\text{fric}} = \frac{f_{fo} G^2 z}{2\rho_f D_h} \left[\frac{1}{x_{eq}} \int_0^{x_{eq}} \phi_{fo}^2 dx_{eq} \right] \quad (1.8)$$

$$-(\Delta p)_{\text{accel}} = \frac{G^2}{\rho_f} \left[\frac{x_{eq}^2}{\alpha} \frac{\rho_f}{\rho_g} + \frac{(1-x_{eq})^2}{1-\alpha} - 1 \right] \quad (1.9)$$

$$-(\Delta p)_{\text{grav}} = \frac{gz \sin\theta}{x_{eq}} \left[\int_0^{x_{eq}} \{ \rho_g \alpha + \rho_f (1-\alpha) \} dx_{eq} \right] \quad (1.10)$$

Evaluation of the terms in brackets in equations (1.8) through (1.10) is the object of the Martinelli-Nelson and Baroczy correlations which are reviewed in Appendix A.

1.2.3 Mixture Model

In order to account for the relative motions of each phase, Zuber [24] developed the mixture field equations in terms of the mixture variables. These were used in (10) to analyze transient phenomena in two-phase mixtures. By neglecting the capillary force, and for steady state flow, the time-smoothed and area-averaged equations are

the continuity equation of the mixture

$$\frac{\partial}{\partial z}(\rho_m v_m) = 0 \quad (1.11)$$

and the momentum equation for the mixture

$$-\left(\frac{dp}{dz}\right)_{\text{total}} = \rho_m v_m \frac{\partial v_m}{\partial z} + g\rho_m + \frac{f_m}{2D_h} \rho_m v_m^2 + \frac{\partial}{\partial z} \left\{ \frac{\rho_f - \rho_m}{\rho_m - \rho_g} \frac{\rho_g \rho_f}{\rho_m} \bar{V}_{gj}^2 \right\} \quad (1.12)$$

where the mixture density is

$$\rho_m = (1-\alpha)\rho_f + \alpha\rho_g \quad (1.13)$$

the mixture velocity is

$$v_m = \frac{(1-\alpha)\rho_f v_f + \alpha\rho_g v_g}{\rho_m} \quad (1.14)$$

and the void fraction is

$$\alpha = \frac{A_g}{A} \quad (1.15)$$

The first and last terms of equation (1.12) are point values and may be integrated directly to give

$$\begin{aligned} -\Delta p_{\text{accel}} &= \rho_m v_m (v_{m_e} - v_{m_o}) \\ &= \frac{G^2}{\rho_f} \frac{\alpha_e \Delta \rho}{\rho_{m_e}} \end{aligned} \quad (1.16)$$

$$-\Delta p_d = \frac{\rho_{f_e} - \rho_{m_e}}{\rho_{m_e} - \rho_{g_e}} \frac{\rho_{f_e} \rho_{g_e}}{\rho_{m_e}} \bar{V}_{gj}^2 \quad (1.17)$$

where \bar{V}_{gj} is the weighted mean drift velocity for upward bubbly churn flow

$$\bar{V}_{gj} = 1.41 \left[\frac{\sigma g \Delta \rho}{2 \rho_f} \right]^{1/4} \quad (1.18)$$

and where ρ_f and ρ_g are the saturation densities corresponding to the system pressure of the liquid and vapor phases respectively. This is a simplifying assumption which is also utilized in the homogeneous, Martinelli-Nelson, and Baroczy models, as outlined in Section 1.2.1.

Integration of the second and third terms is simplified by the above assumption of constant fluid densities. However, additional equations are still required for the void fraction, α , and the mixture friction factor, f_m . The equations which were used to predict these parameters are [12]

$$\langle \alpha \rangle = \frac{x}{C_o \left[\frac{x \Delta \rho}{\rho_f} + \frac{\rho_g}{\rho_f} \right] + \frac{\rho_g V g j}{G}} \quad (1.19)$$

and, the mixture friction factor [4]

$$f_m = f_f \frac{\rho_m}{\rho_f} \left(\frac{1-x}{1-\alpha} \right)^2 \quad (1.20)$$

Use of this expression for the mixture friction factor was jointly suggested by Armand, Lottes, and Levy [4]. Their method is discussed in more detail in Appendix A.

Upon substitution of the equations, numerical integration of the second and third terms of equation (1.12) was accomplished on the Univac 1108 by using the midpoint

rule. Integration was obtained by an iteration technique which was terminated when successive iterations agreed to within $\pm 1/2$ of 1%.

1.3 Purpose

The purpose of Part I of this thesis is to obtain reliable experimental data on pressure drop in two-phase flows with evaporation, and to evaluate the methods of prediction which were discussed in the previous section against these data.

CHAPTER II

EXPERIMENTAL PROGRAM

2.1 Method of Experiments

The apparatus used to obtain pressure drop data is the Freon loop in the School of Mechanical Engineering. A detailed description of the experimental apparatus can be found in [18].

The objective of the experiments was to obtain steady state two-phase flow data of high voidage ($\alpha = .02 \rightarrow .50$) over a significant portion of the test section. Hence, the inlet subcooling for all experimental runs was held as low as possible.

For accurate data, it was important to assure that the flow at the inlet to the test section was single-phase liquid, because at certain pressures it is possible to flash the working fluid within the preheaters of the experimental apparatus. Single-phase liquid was insured for all experimental runs by a preliminary experiment, the purpose of which was to raise the liquid temperature within the test section by the application of a wall heat flux. The wall heat flux was held below that which would induce evaporation within the test section. The measured temperature difference of the inlet and exit liquid was then compared to the theoretical

temperature rise attributable to the applied wall heat flux.

$$\Delta T = \frac{q''_w \xi L}{W c_{p_f}}$$

For agreement of the two temperature differences within 1°F, single phase liquid flow at the inlet was assumed.

Except for high and low Reynolds number comparisons, mass flux for all experiments was set at approximately 10^6 lbm/ft²-hr, which applies to practical systems [20]. Beginning with a low heat flux, steady state flow was achieved (as indicated by the constancy of flow meter readings, wall temperature measurements, and fluid measurements at the exit). At steady state flow, pressure drop measurements were then recorded at one foot intervals along the test section. This procedure was repeated for larger heat flux application until it was no longer possible to sustain steady state flow (as indicated by an oscillation in flow meter readings of greater than $\pm 5\%$).

Data were obtained at system pressures of 150, 175, and 195 psia for a mass flux of 10^6 lbm/ft²-hr. This corresponds to an inlet Reynolds number of 65,000. For an investigation of the Reynolds number effect, data were obtained at a system pressure of 175 psia and an inlet Reynolds number of 115,606, and also at a system pressure of 195 psia and an inlet Reynolds number of 30,121. It was necessary to obtain the low Reynolds number data at the

highest system pressure due to flashing of the fluid within the preheaters at reasonable subcooling ($<80^{\circ}\text{F}$) and lower pressures.

2.2 Accuracy of Data

Detailed description of the Freon Loop of the School of Mechanical Engineering can be found in [18]. Accuracy of the recording instruments used are

Flow Meter	$\pm 0.25\%$ of reading to normal maximum rated flow
Flow Rate Indicator	$\pm 0.10\%$ full scale
System Pressure Gage	$\pm 0.25\%$ of reading to maximum pressure tolerance
Digital Voltmeter	$\pm 0.1\%$ of reading
Ammeter	$\pm 2\%$ (2 amps in 120)
Temperature Recorder	$\pm 1^{\circ}\text{F}$

In order to assure consistency of data, the runs for the high Reynolds number data at 175 psia were repeated. These two different runs, at the same experimental conditions can be compared in Tables 10 through 19 in Appendix B and Figure 10 in Chapter III. It is shown that data repeatability of the experimental apparatus is assured.

CHAPTER III

RESULTS AND DISCUSSION

Figures 2 through 7 summarize the results of the homogeneous, Martinelli-Nelson, Baroczy, and Armand-Lottes-Levy models in predicting the total pressure drop in two-phase flows. Tables which list all data shown in these figures are located in Appendix B.

For these data, the magnitude of experimental pressure drop is indicative of the length of the two-phase flow regime along the channel. Hence, the reason for good predictive agreement at low levels of experimental pressure drop is that the frictional component of the total pressure drop is small. From the data, it is readily seen that as the heat flux is increased (thereby increasing the two-phase flow regime within the channel), the predicted pressure drop deviates more from the experimental value. This is especially apparent from the high inlet Reynolds number runs. Therefore, the data confirm the fundamental deficiency of the various predictive methods, i.e., an accurate model for representation of frictional losses at the wall is not available today.

Another result which was derived from the experimental data is represented in Figures 8 and 9. These are plots of

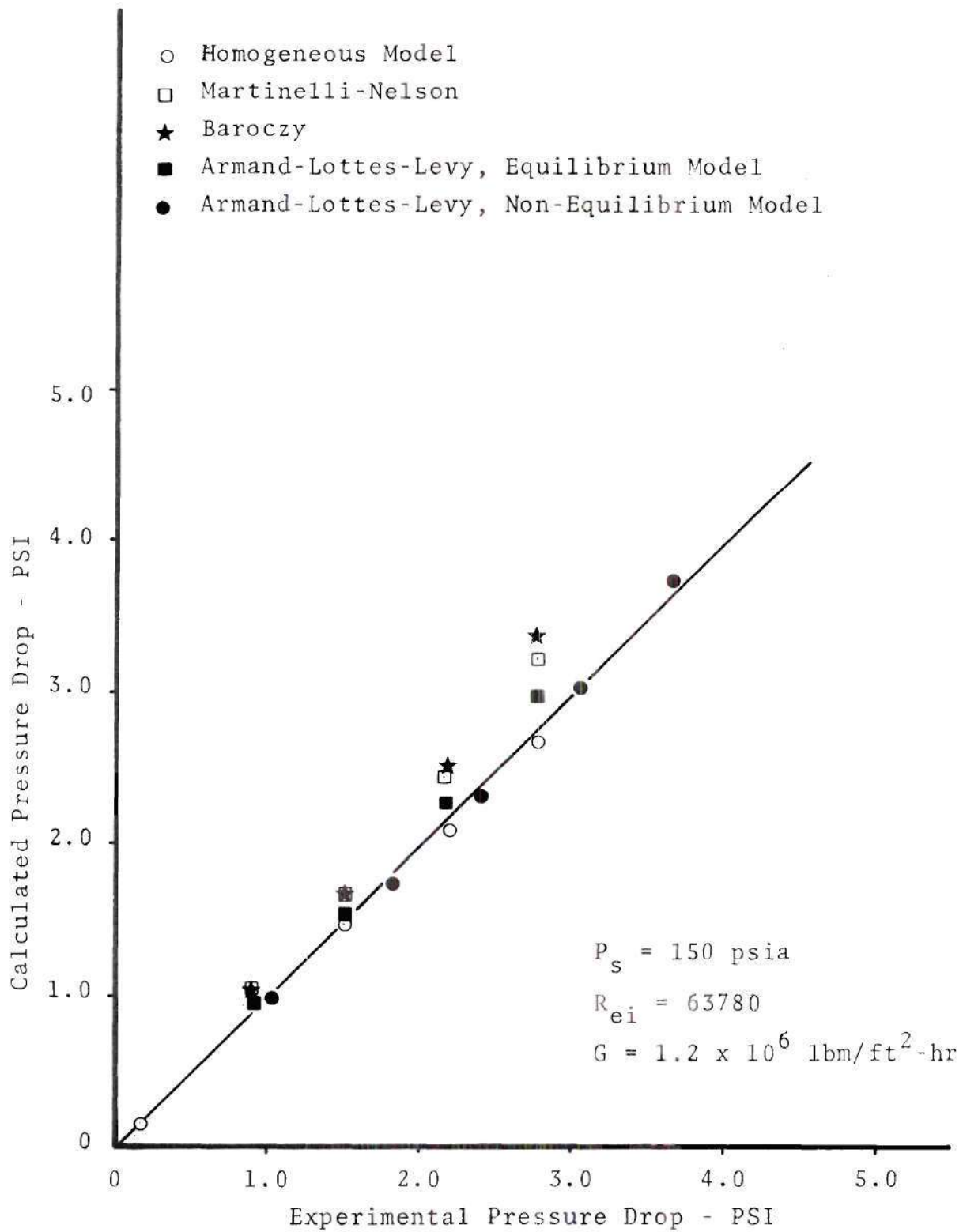


Figure 2. Pressure Drop Estimation in Two-Phase Flow with Evaporation

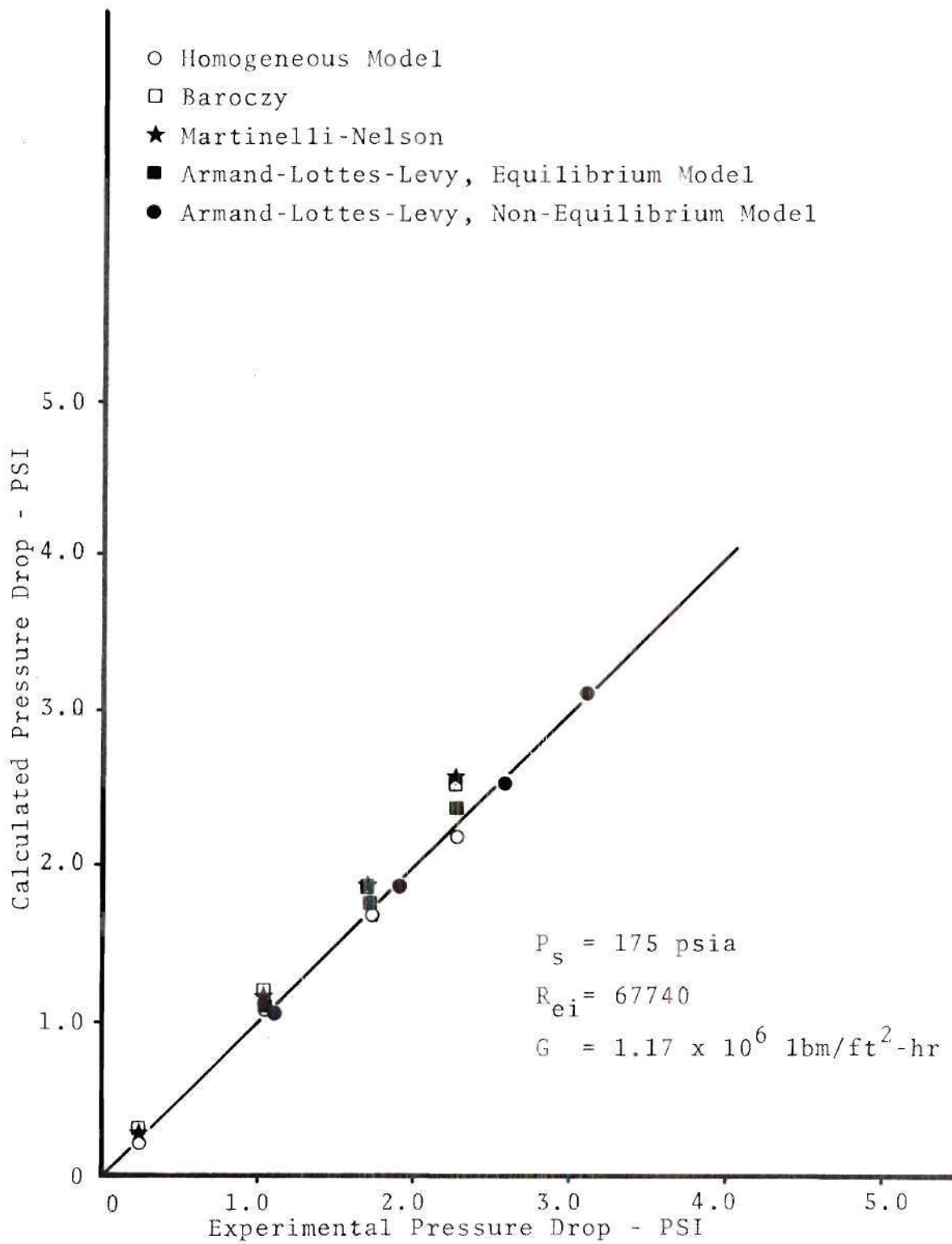


Figure 3. Pressure Drop Estimation in Two-Phase Flow with Evaporation

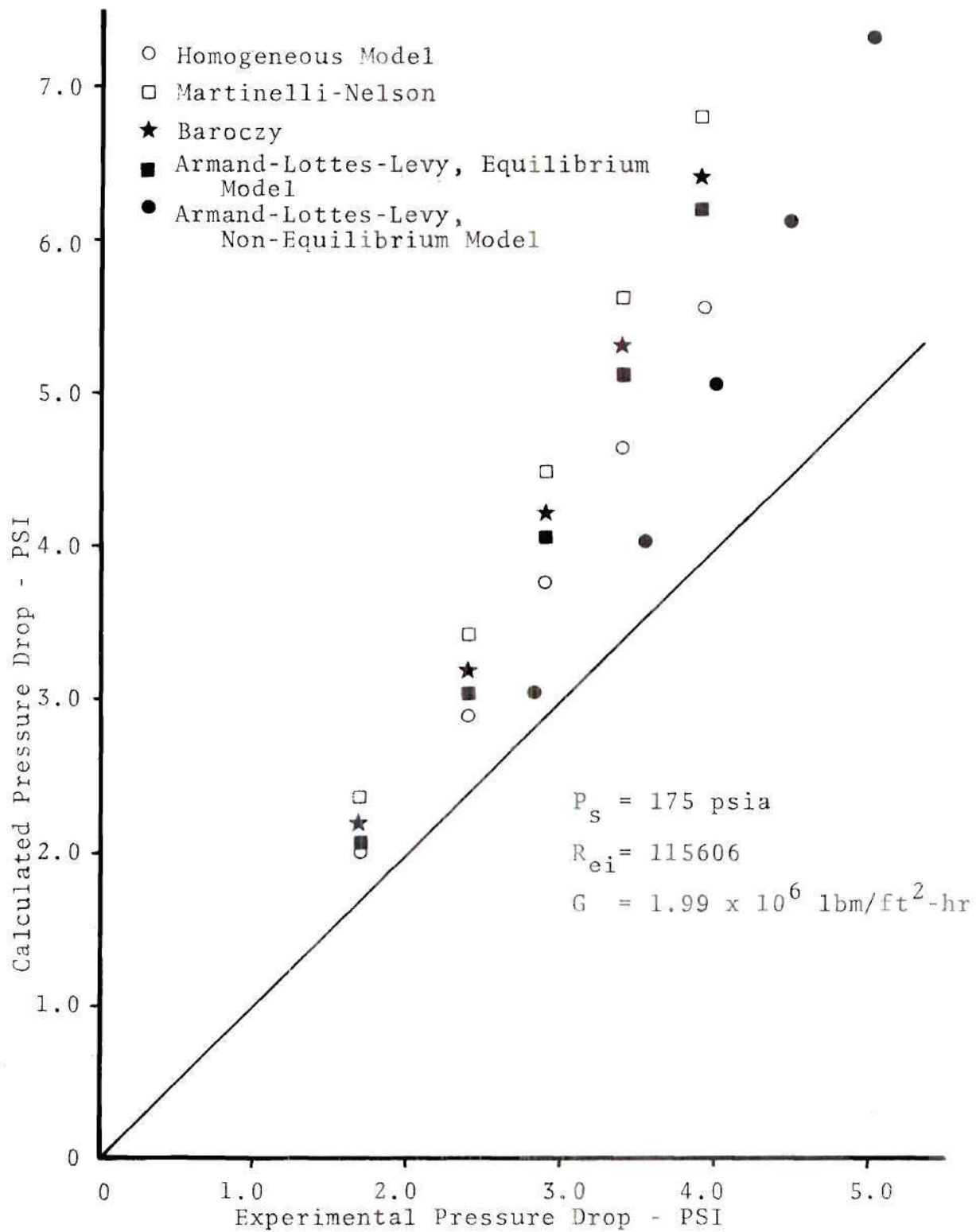


Figure 4. Pressure Drop Estimation in Two-Phase Flow with Evaporation

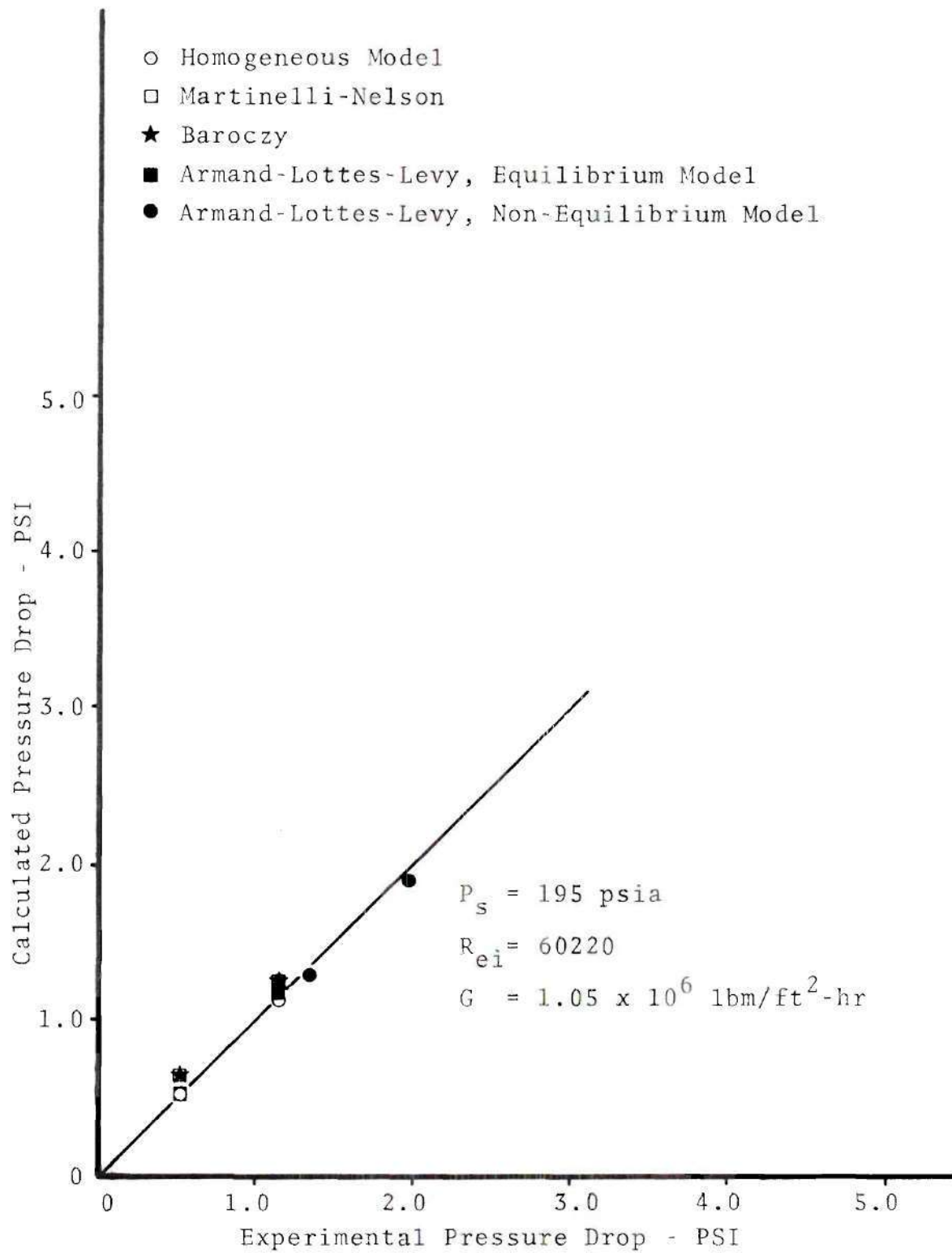


Figure 5. Pressure Drop Estimation in Two-Phase Flow with Evaporation

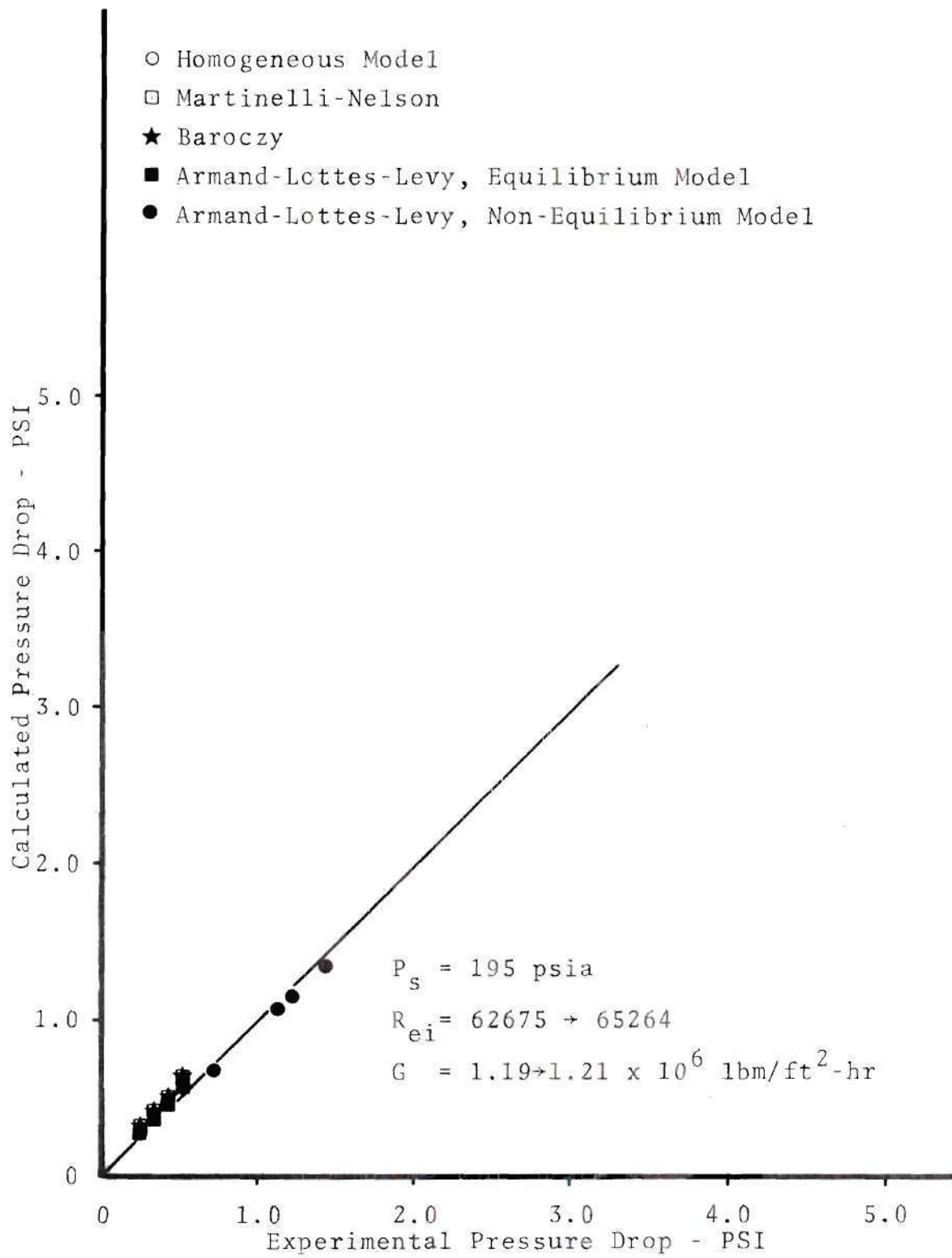


Figure 6. Pressure Drop Estimation in Two-Phase Flow with Evaporation

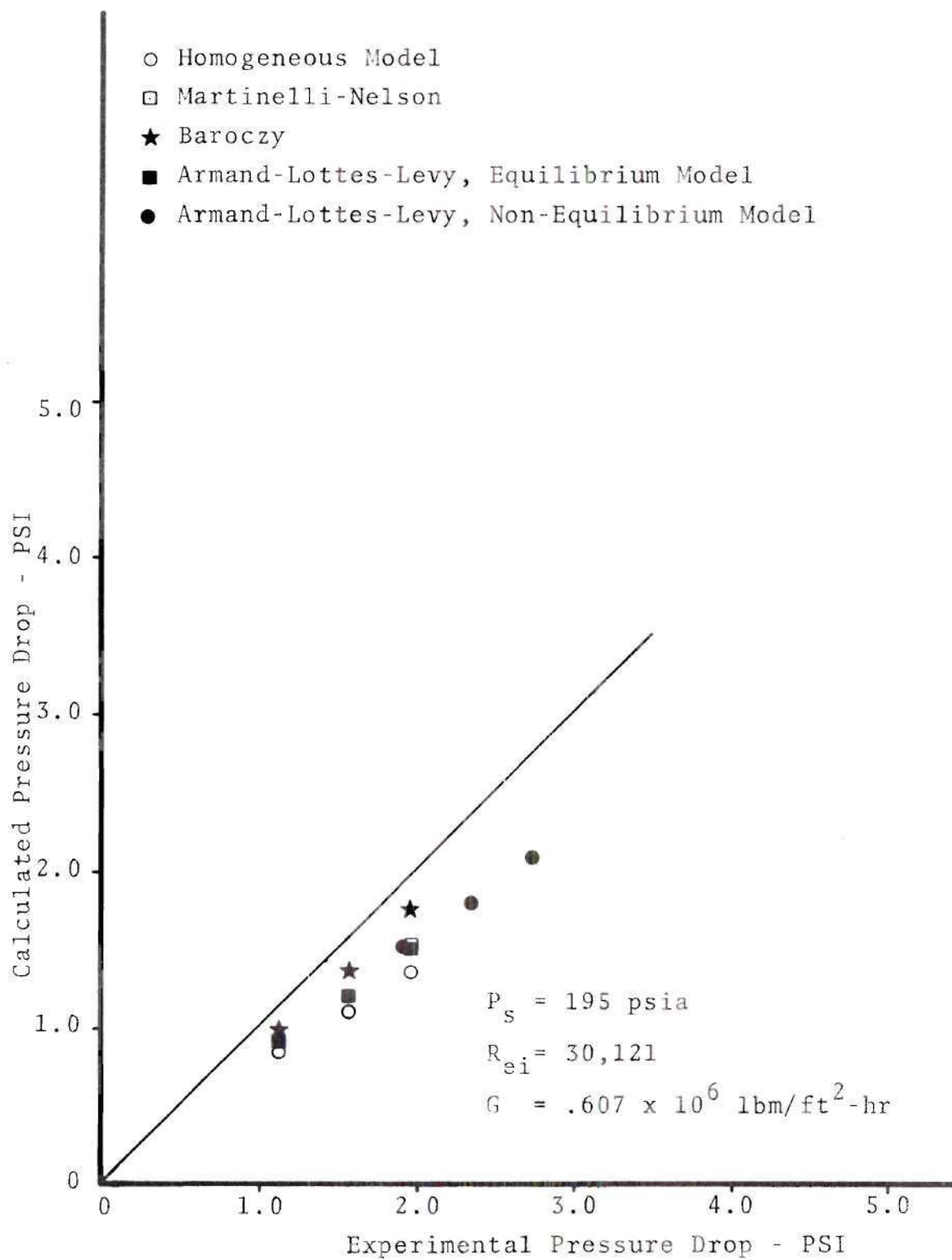


Figure 7. Pressure Drop Estimation in Two-Phase Flow with Evaporation

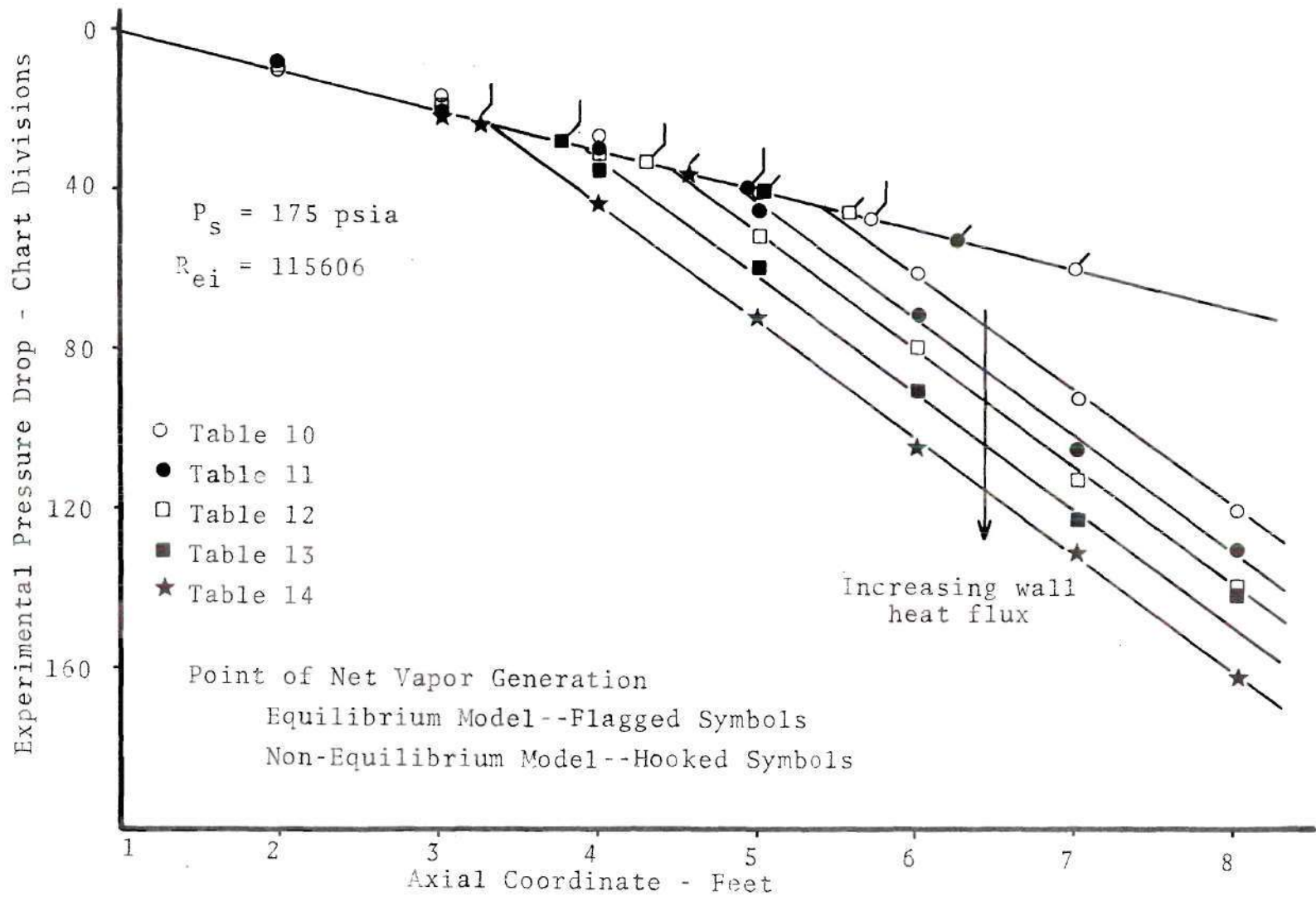


Figure 8. Increase of Experimental Pressure Drop with Onset of Nucleation (Chart Divisions)

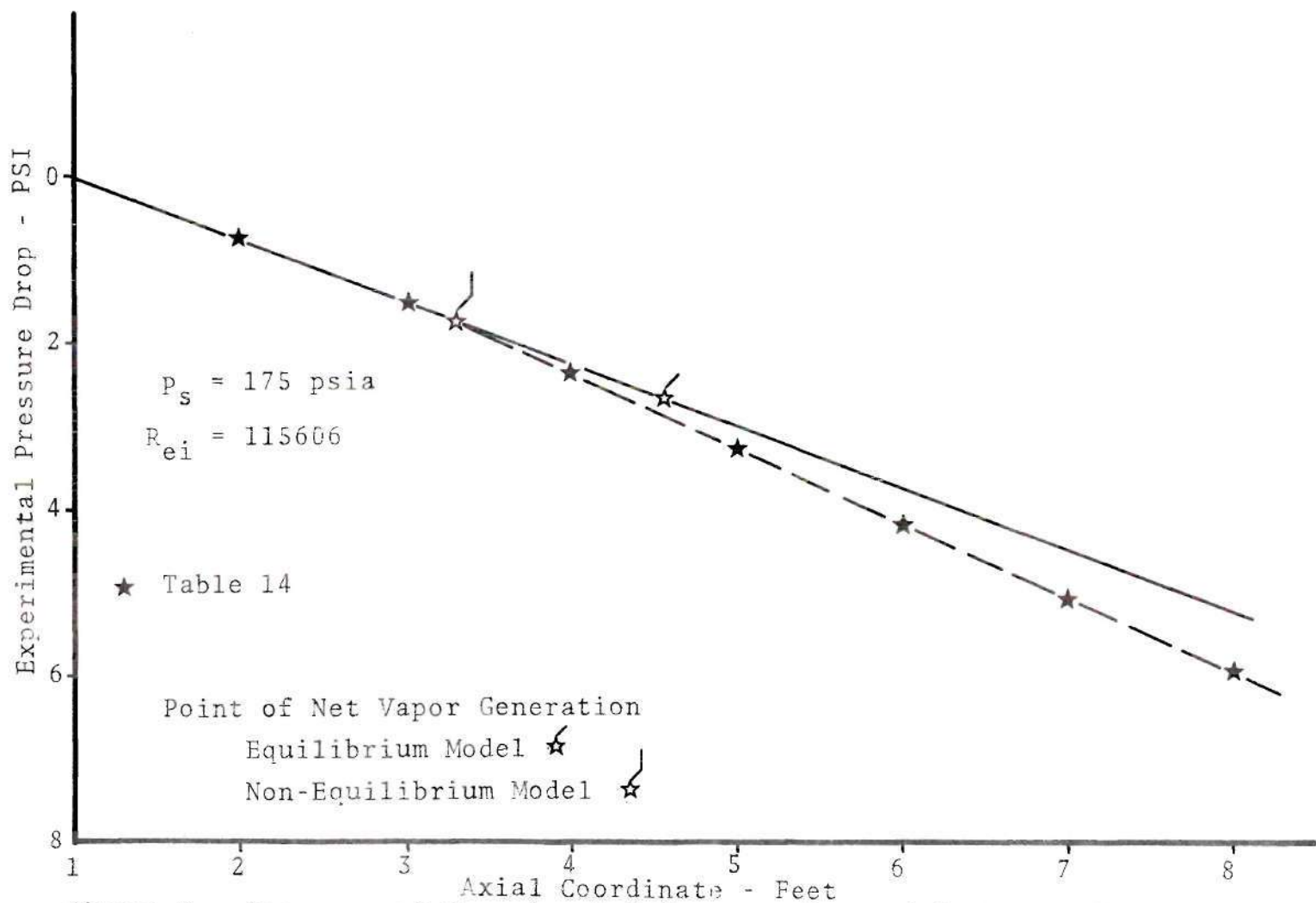


Figure 9. Increase of Experimental Pressure Drop with Onset of Nucleation (Actual PSI)

pressure drop between a reference location in the channel, one foot downstream of the inlet, and a point in the channel, versus axial position. The figures show a constant pressure gradient between the reference point and some location within the channel where it increases abruptly. This phenomenon is indicative of bubble nucleation at the wall, that is, of subcooled boiling, and hence an increased friction factor. Also shown on these plots is a prediction of the point of net vapor formation from [19] (non-equilibrium theory summarized in Appendix A), and the point of initiation of two-phase flow as predicted by equilibrium theory. It can be seen that the non-equilibrium theory of [19] is in good agreement with experimental data, whereas use of the equilibrium model for predicting the point of net vapor formation is in error.

Since the two-phase friction factor is greater than the corresponding single phase friction factor, due to the roughness presented by nucleating bubbles, it is evident that use of a single phase friction factor will result in an underestimation of frictional pressure drop. Hence, for pipes where transition from single-phase to two-phase flow occurs, current practice of utilizing equilibrium theory to define the point of transition will result in an underestimation of pressure drop within the single phase region, due to the effects of thermal non-equilibrium. This result is verified by the data presented in Figures 8 and 9.

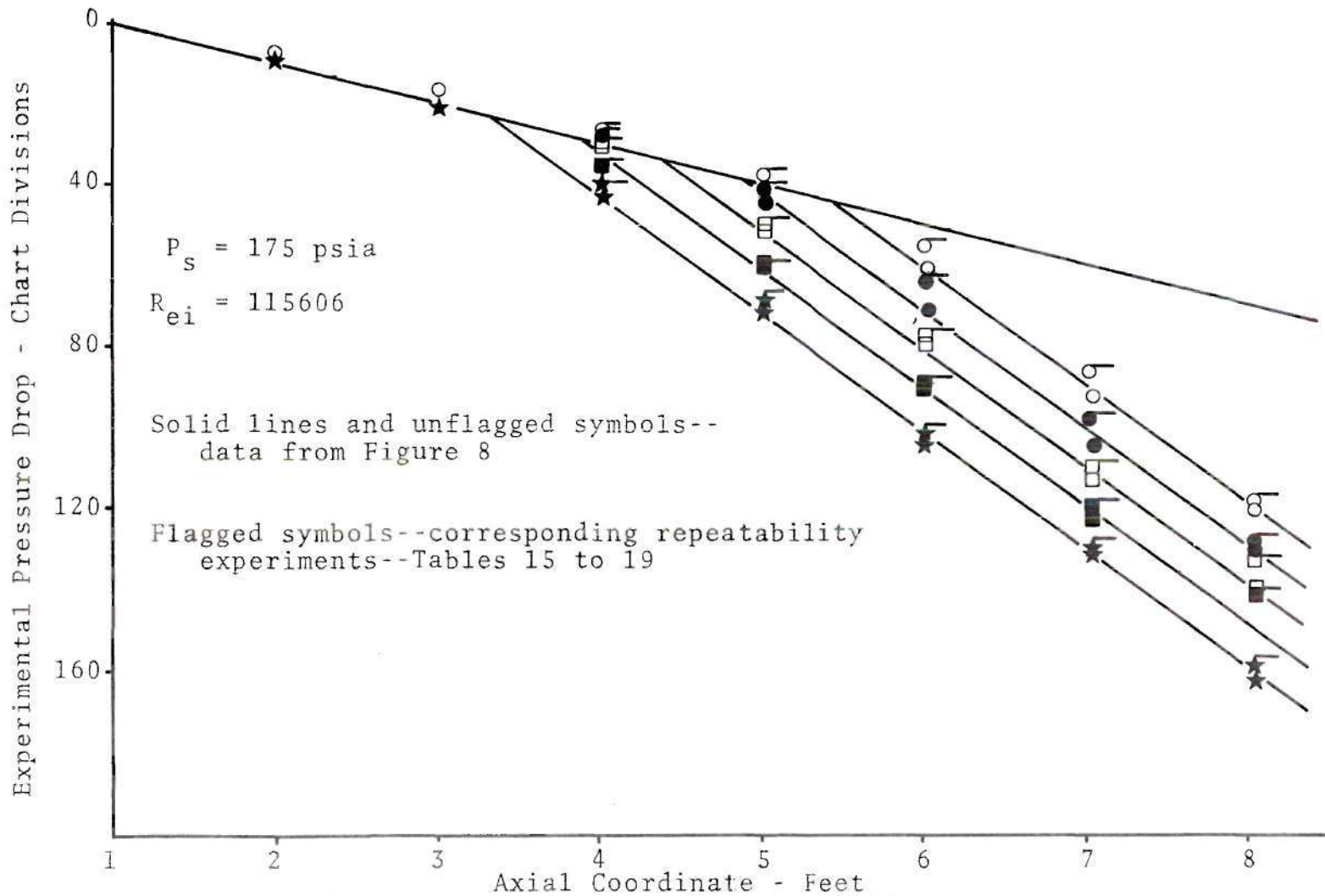


Figure 10. Experimental Repeatability

CHAPTER IV

CONCLUSIONS

The following conclusions are drawn from the experimental data:

(1) The heretofore proposed correlations to predict two-phase flow pressure drop are inaccurate and inconsistent when applied to the data obtained from the present experiments.

(2) The primary reason for inaccuracy of the various predictive methods is failure to properly model the frictional component of pressure drop.

(3) The equilibrium model of predicting the point of net vapor formation is in error for practical applications, and results in underestimation of frictional pressure drop in the single-phase region as predicted by equilibrium theory.

(4) Hence, a non-equilibrium model for prediction of void fraction and mass quality is required.

Part II
A CONSTITUTIVE EQUATION FOR THE
NET RATE OF VAPOR GENERATION
IN SUBCOOLED BOILING

CHAPTER I

INTRODUCTION

1.1 Significance of the Problem

As was outlined in Part I of the present thesis, the ability to predict pressure drop in non-adiabatic, non-equilibrium flows is incumbent upon the accurate estimation of the functional relationship of void fraction with axial position. In addition, the rate of vapor formation may affect the thermo-hydraulic behavior of the system. In particular, the question arises whether the density, velocity, pressure, and thermal fields may interact in such a way so as to give rise to

- a) excursions in both flow and temperature
- b) oscillations in flow velocity, temperature, density, and pressure
- c) choking flows.

The appearance of any of the above phenomena may define the operating limits of non-adiabatic two-phase flow systems. It has been shown that the traditional approach to the problem (i.e., assumption of thermodynamic equilibrium between the phases) may be inadequate for certain operating conditions since local vapor void fractions as high as 30% have been measured under conditions of thermal non-equilibrium,

for example, in the region of subcooled boiling. Hence, a general non-equilibrium approach is needed in order to properly analyze proposed upratings of such systems.

1.2 Purpose

The present analysis has two objectives: (1) to consider the general characteristics of thermal non-equilibrium two-phase flows, and (2) to develop a constitutive equation which specifies the net rate of vapor formation for a particular thermal non-equilibrium two-phase flow system, that is, for vapor generation in subcooled boiling.

The analysis will be developed from a model which can be applied to transient as well as to steady state operating conditions.

CHAPTER II

PRESENT STATE OF THE ART

In order to discuss both the problems of thermal equilibrium and non-equilibrium, it is instructive to consider the generalized time smoothed and area averaged

continuity equation of the vapor [11]

$$\frac{\partial}{\partial t} (\alpha \rho_g) + \frac{\partial}{\partial z} (\alpha \rho_g v_g) = \Gamma_g \quad (2.1)$$

and the energy equation of the mixture [11]

$$(1-\alpha) \rho_f \left[\frac{\partial i_f}{\partial t} + v_f \frac{\partial i_f}{\partial z} \right] + \alpha \rho_g \left[\frac{\partial i_g}{\partial t} + v_g \frac{\partial i_g}{\partial z} \right] + \Gamma_g (i_g - i_f) = \frac{\dot{q}''_w \xi}{A} + \frac{\partial p}{\partial t} \quad (2.2)$$

where the effects of kinetic and potential energies have been neglected.

The first two terms on the left hand side of equation (2.2) account for the thermodynamic non-equilibrium of the liquid and of the vapor respectively. The third term is the energy required to generate a mass of vapor per unit volume

per unit time, Γ_g . In general, Γ_g must be specified by a constitutive equation. The first term on the right hand side accounts for the power input per unit volume. The second term accounts for the effects of system pressure variations on the energy content.

Generally, the right hand side of equation (2.2) is known, whereas the left hand side is not. That is, for a given energy input to the two-phase mixture, it is not known which proportion is utilized to produce vapor, or which proportions go to heat the liquid and/or vapor (either of which may be superheated or subcooled).

2.1 Characteristics of Thermal Equilibrium Flow

For a mixture in thermal equilibrium, the fluid enthalpies remain constant at the local system pressure, whereas the entire energy input to the mixture is utilized without time delay to vaporize the liquid. Furthermore, if it is assumed that the pressure drop is small compared to the total system pressure, the fluid enthalpies may be approximated as being constant throughout the entire channel, and the rate of vapor formation, Γ_g , may be computed directly from equation (2.2), thus

$$\Gamma_{eq} = \frac{\dot{q}''_w \xi}{A \Delta i_{fg}} \quad (2.3)$$

if the effect of temporal pressure variation is neglected.

Substitution of (2.3) into the steady state form of (2.1) results in the standard expression, that is, in the definition of the gradient of the equilibrium quality, thus

$$\frac{1}{G} \frac{\partial}{\partial z} (\alpha \rho_g v_g) = \frac{1}{G} \frac{\partial G_g}{\partial z} = \frac{\partial x_{eq}}{\partial z} = \frac{\dot{q}''_w \xi}{GA \Delta i_{fg}} \quad (2.4)$$

Since the fluid enthalpies are constant for the thermal equilibrium model, there is no time delay in transferring the energy from the wall to the vapor-liquid interface. Hence, no information of the heat transfer process from the wall to the interface is required. Clearly then, no consideration of the flow regime is necessary. The mechanism of heat transfer from the heated solid surface to the vapor-liquid interface can be considered only in conjunction with the flow regime. This latter point is the characteristic of non-equilibrium flows, and is discussed below.

2.2 Characteristics of Thermal Non-Equilibrium Flow

As stated previously, it is not generally known which proportion of the wall heat flux is utilized to produce vapor, or which proportions go toward heating the liquid and/or vapor (either of which may be superheated or subcooled). It has been shown in [22] that the degree of thermal non-equilibrium depends on the rate of vapor formation per unit volume, Γ_g , which must be specified for the various

flow regimes by a constitutive equation. In order to illustrate this fact (and following reference [22]), three cases of thermal non-equilibrium flows will be considered.

2.2.1 Superheated Liquid Only ($\alpha=0, \Gamma_g=0$)

For a flowing superheated liquid in the absence of a vapor phase, equation (2.2) shows that the entire energy input to the system (due to heat input and/or pressure variations) is used to increase the enthalpy of the liquid. Hence, any enthalpy increase above saturation will result in the storage of energy in a thermodynamically unstable state. From this it is evident that, if, at a subsequent time, vapor bubbles are nucleated, their rate of growth will depend on the amount of liquid superheat.

2.2.2 Bubbly Flow--Superheated Liquid with Vapor Bubbles

($\alpha \neq 0, \Gamma_g \neq 0, i_g = \text{constant}$)

For the case where the vapor enthalpy remains constant at the saturation value, equation (2.2) indicates that part of the energy which is transferred to the mixture is used to increase the enthalpy of the liquid, i_f , whereas the other portion, $\Gamma_g(i_{g,sat} - i_f)$, is used for vapor generation. Hence, the degree of thermal non-equilibrium depends upon the mass rate of vapor formation, Γ_g .

For vapor bubbles in a superheated liquid, Γ_g will depend on (a) the rate at which bubbles will nucleate, and (b) the rate at which bubbles will grow. The latter rate depends upon the rate at which energy is transferred to the

vapor-liquid interface. Note, that this heat transfer rate depends on (a) the geometry of the interface, (b) the transport properties of the liquid, and (c) the thermal and flow fields in the liquid in the vicinity of the vapor-liquid interface.

2.2.3 Bubbly Flow--Subcooled Liquid with Vapor Bubbles

$(\alpha \neq 0, \Gamma_g \neq 0, i_g = \text{constant})$

As in the previous example, equation (2.2) indicates that a part of the energy which is transferred to the mixture is used to increase the enthalpy of the liquid, i_f , whereas the remainder, $\Gamma_g(i_{g,\text{sat}} - i_f)$, is used for vapor generation. However, the characteristics of this type of flow are different in that bubbles nucleate in a thin layer of superheated liquid film near the wall and collapse in the bulk subcooled liquid. Therefore, the amount of vapor present depends upon the rate of vapor generation, that is, heterogeneous nucleation, as well as on the processes of evaporation and condensation.

Flows other than those considered above are discussed in reference [22]. However, it can be seen from this brief discussion that the rate of vapor generation per unit volume, Γ_g , determines the degree of thermal non-equilibrium.

2.3 The Formal Approach

The formal approach to the problem of thermal non-equilibrium flows has been discussed in [3,12,23]. For

a bubbly flow through a duct of constant cross section, the mass flow rate of vapor passing the axial coordinate z is given by

$$G_g(z) = \frac{\xi}{A} \int_{\lambda}^z m(z, z') J(z') dz' \quad (2.5)$$

where

$m(z, z')$ = mass of bubble at z that nucleated at z' ,
and which contributes to the vapor flux
at z .

$J(z')$ = rate of bubble nucleation per unit area
at z'

Differentiation of equation (2.5) results in the mass rate of vapor formation per unit volume Γ_g

$$\Gamma_g(z) = \frac{dG_g}{dz} = \frac{\xi}{A} \int_{\lambda}^z \frac{dm(z, z')}{dz} J(z') dz' \quad (2.6)$$

The main problem associated with using the formal approach to the thermal non-equilibrium problem is that there is no accurate model available today with which to obtain (a) the rate of heterogeneous nucleation, $J(z')$, (b) the nucleating characteristics of the surface which affect $J(z')$, and (c) the bubble growth and/or collapse law, $m(z, z')$. Because of these difficulties, two approximation methods have been used in the literature. These are considered below.

2.4 Approximation Methods

For the case of subcooled boiling, and by assuming that the vapor is at saturation, that is, in thermal equilibrium, equations (2.1) and (2.2) for steady state flow reduce to

$$\frac{\partial}{\partial z} (\alpha \rho_g v_g) = G \frac{dx}{dz} = \Gamma_g \quad (2.7)$$

$$(1-\alpha) \rho_f v_f \frac{\partial i_f}{\partial z} + \Gamma_g (i_{g,sat} - i_f) = \frac{\dot{q}''_w \xi}{A} \quad (2.8)$$

It is noted that the quality, x , in equation (2.7) is the true quality and not that which corresponds to thermal equilibrium as defined by equation (2.4).

It should be noted also that in equation (2.7) neither x nor Γ_g are known, whereas in equation (2.8) the liquid enthalpy, i_f , and Γ_g are unknown. Thus, only two equations are available which contain three unknown variables. The problem could be closed with the specification of an appropriate constitutive equation of evaporation, Γ_g . However, because of the difficulties (noted in the preceding section) in specifying Γ_g , previous approaches were formulated by assuming either a liquid enthalpy distribution in equation (2.8), references [1,12,18] or a quality distribution in equation (2.7), reference [13]. Both of these approaches to the problem will be briefly reviewed.

By considering the boundary conditions which the steady state enthalpy of the liquid must satisfy, that is

$$\begin{aligned} \text{at } z = \lambda, \quad i_f = i_\lambda \quad \text{and} \quad \frac{di_f}{dz} = \frac{i_{f,\text{sat}} - i_\lambda}{\lambda_{\text{eq}}^{-\lambda}} = \frac{\Delta i_\lambda}{\Delta \ell} \\ \text{at } z \rightarrow \infty, \quad i_f \rightarrow i_{f,\text{sat}} \quad \text{and} \quad \frac{di_f}{dz} \rightarrow 0 \end{aligned} \quad (2.9)$$

The authors of references [12,18] postulated the following axial enthalpy distribution

$$\frac{i_f(z) - i_\lambda}{i_{f,\text{sat}} - i_\lambda} = 1 - \exp\left\{-\frac{z - \lambda}{\Delta \ell}\right\} = 1 - \exp\left\{-\frac{i(z) - i_\lambda}{i_{f,\text{sat}} - i_\lambda}\right\} \quad (2.10)$$

where the length, $\Delta \ell$, is given by

$$\Delta \ell = \lambda_{\text{eq}}^{-\lambda} = \frac{GA(i_{f,\text{sat}} - i_\lambda)}{q''_w \xi} \quad (2.11)$$

From equation (2.10), and the definitions of quality

$$x = \frac{i(z) - i_f(z)}{i_g(z) - i_f(z)} \quad (2.12)$$

and of equilibrium quality

$$x_{\text{eq}} = \frac{i(z) - i_{f,\text{sat}}}{\Delta i_{fg}} \quad (2.13)$$

the following expression for vapor quality in subcooled boiling was derived in [12]

$$x = \frac{x_{eq} + \frac{c_p \Delta T_{sub}}{\Delta i_{fg}} \exp\left\{-\frac{x_{eq} \Delta i_{fg}}{c_p \Delta T_{sub}} - 1\right\}}{1 + \frac{c_p \Delta T_{sub}}{\Delta i_{fg}} \exp\left\{-\frac{x_{eq} \Delta i_{fg}}{c_p \Delta T_{sub}} - 1\right\}} \quad (2.14)$$

More recently, Saha [18] derived the following expression for the net rate of vapor generation

$$\Gamma_g = \frac{\dot{q}''_w \xi}{A \Delta i_{fg}} \{1 - \exp[-\frac{z-\lambda}{\Delta \ell}]\} \quad (2.15)$$

which was obtained from equations (2.8) and (2.10) by introducing the simplifying assumptions

$$(1-x) \frac{di_f(z)}{dz} \approx \frac{di_f(z)}{dz} \quad (2.16)$$

and

$$\Delta i_{fg} + i_{f,sat} - i_\lambda \approx \Delta i_{fg} \quad (2.17)$$

This expression for Γ_g was successfully used in reference [18] to analyze the onset of thermally induced flow

oscillations in boiling two-phase mixtures.

The second approach, that is, of specifying a quality distribution was introduced by Levy [13]. In evaluating the effects of thermal non-equilibrium, Levy postulated the following quality distribution

$$x = x_{eq} + \frac{c_p \Delta T_{sub}}{\Delta i_{fg}} \exp\left\{-\frac{x_{eq} \Delta i_{fg}}{c_p \Delta T_{sub}} - 1\right\} \quad (2.18)$$

based upon the reasoning that it satisfied the following boundary conditions

$$\text{at } z = \lambda, x = 0 \quad (2.19)$$

$$\text{at } z \rightarrow \infty, x \rightarrow x_{eq} \quad (2.20)$$

It is noted that if the denominator in equation (2.14) is approximated by unity then equations (2.14) and (2.18) become identical. For most cases in practical applications this approximation is valid.

It was shown in [12,18,23] that both approaches, that is, equation (2.14) and equation (2.18) when applied to subcooled boiling were successful in predicting the steady state vapor void fraction.

As can be seen, the approximation methods discussed above can be justified only for the case of steady state flow.

For the purpose of analyzing system oscillations, or excursions in both flow and temperature, the above approach is incomplete since the temporal variation of temperature distribution is not known for transient flows. This is the basic shortcoming which is common to all previous attempts at specifying the constitutive equation of net vapor formation.

2.5 Conclusions

The following conclusions are drawn from the preceding discussion.

(a) The mass rate of vapor generation per unit volume, Γ_g , determines the degree of thermal non-equilibrium and furthermore, depends upon the flow regime.

(b) A constitutive equation to predict Γ_g is not available in the literature. Instead, two approximation methods have been used. One is based upon an assumed liquid enthalpy distribution, and the other is based upon an assumed quality distribution.

(c) Both approximation methods were based upon steady state considerations.

CHAPTER III

FORMULATION

The purpose of the analysis presented below is to develop a model which can be used to predict the net mass rate of vapor formation per unit volume in both transient and steady-state, thermal non-equilibrium (subcooled boiling), two-phase flow. The model is based upon a specific constitutive equation of evaporation, Γ_g . The selection of the particular expression for Γ_g is guided by the traditional approach to chemical rate processes.

3.1 Model

The model considered is that for homogeneous flow. Hence, the velocities of the vapor and of the liquid are equal, and the following set of field equations govern the flow

the continuity equation of the vapor

$$\frac{\partial}{\partial t} (\rho x) + \frac{\partial}{\partial z} (\rho x v) = \Gamma_g \quad (3.1)$$

the continuity equation of the mixture

$$\frac{\partial \rho}{\partial t} + \frac{\partial}{\partial z} (\rho v) = 0 \quad (3.2)$$

the energy equation of the mixture

$$\rho \left\{ \frac{\partial i}{\partial t} + v \frac{\partial i}{\partial z} \right\} = \frac{\dot{q}''_w \xi}{A} + \frac{\partial p}{\partial t} \quad (3.3)$$

and the momentum equation of the mixture

$$\rho \left\{ \frac{\partial v}{\partial t} + v \frac{\partial v}{\partial z} \right\} = - \frac{\partial p}{\partial z} - \frac{\partial \tau}{\partial z} + g \rho \quad (3.4)$$

where the effects of kinetic energy and potential energy have been neglected. In addition, the following definitions apply to homogeneous flow

the density of the mixture

$$\frac{1}{\rho} = \frac{1-x}{\rho_f} + \frac{x}{\rho_g} \quad (3.5)$$

where the fluid densities are specified by the appropriate thermal equations of state

$$\rho_f = \rho_f(p, T_f) \quad \text{and} \quad \rho_g = \rho_g(p, T_g) \quad (3.6)$$

and the enthalpy of the mixture

$$i = (1-x)i_f + xi_g \quad (3.7)$$

where the fluid enthalpies are specified by the appropriate caloric equation of state

$$i_f = i_f(p, T_f) \text{ and } i_g = i_g(p, T_g) \quad (3.8)$$

Finally, the following constitutive equations are required in order to complete the system

the wall heat flux

$$\dot{q}''_w = \dot{q}''_w(G, \dots) \quad (3.9)$$

the rheological equation of state

$$\tau = \tau(G, \dots) \quad (3.10)$$

and the constitutive equation for the net rate of vapor formation per unit volume

$$\Gamma_g = \Gamma_g(i, \dots) \quad (3.11)$$

The specific non-dimensional form of equation (3.11) will be postulated as

$$\frac{d\Gamma^+}{di^+} = 1 - \Gamma^+ \quad (3.12)$$

where the dimensionless liquid enthalpy is defined by

$$i^+ = \frac{i(z) - i_\lambda}{i_{f, \text{sat}} - i_\lambda} \quad (3.13)$$

the dimensionless net rate of vapor generation by

$$\Gamma^+ = \frac{\Gamma_g}{\Gamma_{\text{eq}}} \quad (3.14)$$

and the rate of vapor formation corresponding to thermal equilibrium, Γ_{eq} , is given by equation (2.3). The selection of the form of equation (3.12) was guided by the traditional approach to chemical rate processes and corresponds to a first order rate equation in that approach.

Equations (3.1) through (3.10) and equation (3.12) constitute a set of thirteen equations in fourteen unknowns

$$\rho, x, v, \Gamma_g, i, \dot{q}''_w, p, \tau, \rho_f, \rho_g, i_f, i_g, T_f, T_g$$

Hence, the above set of equations is not closed. For the particular problem of interest (i.e. non-equilibrium, subcooled boiling), the assumption is made that the gas phase enthalpy, i_g , is constant and equal to the saturation value, i.e.

$$i_g = i_{g, \text{sat}} = \text{constant} \quad (3.15)$$

Although this assumption closes the problem, the system of equations remains coupled.

3.2 Decoupling of the Governing Equations

For many problems, in particular, subcooled boiling, the assumption is made of constant fluid densities, i.e.

$$\rho_f = \rho_{f,sat} \text{ and } \rho_g = \rho_{g,sat} \quad (3.16)$$

This simplification is based upon two conditions. Firstly, it has been shown in [10,11] that for low frequency oscillations, fluid densities remain approximately constant. Secondly, for the case where total pressure drop is small compared to the system pressure, the saturation state changes very little. Furthermore, the temperature range of interest for most operating systems is small enough so that the effect of thermal expansion on the liquid is negligible.

For the above assumption, it can be seen from equation (3.5) that the mixture density is then a function of quality only since the constituent fluid densities are constant, i.e.

$$\frac{1}{\rho} = \frac{1}{\rho(x)} = \frac{1-x}{\rho_{f,sat}} + \frac{x}{\rho_{g,sat}} \quad (3.17)$$

Furthermore, for small system pressure variations, i.e.

$$\frac{\partial p}{\partial t} \approx 0 \quad (3.18)$$

the above assumption permits the mixture momentum equation (3.4) to be decoupled from the governing set of equations. Hence, in view of equations (3.15), (3.16), (3.17) and (3.18) the decoupled system becomes

the continuity equation for the vapor

$$\frac{1}{\rho} \frac{D\rho}{Dt} = - \frac{\Gamma_g}{\rho_{g,sat}} \frac{\Delta\rho}{\rho_{f,sat}} \quad (3.19)$$

the continuity equation for the mixture

$$\frac{\partial v}{\partial z} = \frac{\Gamma_g}{\rho_{g,sat}} \frac{\Delta\rho}{\rho_{f,sat}} \quad (3.20)$$

the energy equation for the mixture

$$\rho \frac{Di}{Dt} = \frac{q''_w \xi}{A} \quad (3.21)$$

the density of the mixture

$$\frac{1}{\rho} = \frac{1-x}{\rho_{f,sat}} + \frac{x}{\rho_{g,sat}} \quad (3.17)$$

the wall heat flux

$$\dot{q}''_w = \dot{q}''_w(G, \dots) \quad (3.9)$$

and the constitutive equation for the net rate of vapor formation per unit volume

$$\frac{d\Gamma^+}{di^+} = 1 - \Gamma^+ \quad (3.12)$$

Hence, this is a set of six equations in six unknowns

$$\rho, x, v, \Gamma_g, i, q''_w$$

In what follows, the model presented above, and in particular the constitutive equation for the net rate of vapor formation, equation (3.12), will be solved in order to obtain the density of the mixture and hence the quality of the vapor. With the mixture density and mixture velocity known, the momentum equation, that is, equation (3.4) may then be integrated directly.

In order to test the model, the vapor quality will be used to obtain the void fraction, α , by the method of [12]. The point of net vapor generation, λ , will be predicted by using the general correlation of [18,19].

3.3 Mixture Density and True Vapor Quality

The following quantities are introduced to the analysis

the dimensionless mixture enthalpy

$$i^+ = \frac{i(z) - i_\lambda}{i_{f,sat} - i_\lambda} \quad (3.22)$$

the dimensionless mixture density

$$\rho^+ = \frac{\rho}{\rho_{f,sat}} \quad (3.23)$$

the net rate of vapor formation based upon equilibrium theory

$$\Gamma_{eq} = \frac{\dot{q}''_{w\xi}}{\Delta i_{fg} A} \quad (3.24)$$

the equilibrium frequency of evaporation

$$\Omega_{eq} = \frac{\Gamma_{eq}}{\rho_{g,sat}} \frac{\Delta \rho}{\rho_{f,sat}} \quad (3.25)$$

the dimensionless time

$$t^+ = t \Omega_{eq} \quad (3.26)$$

the dimensionless length

$$z^+ = \frac{z}{L} \quad (3.27)$$

the dimensionless mixture velocity

$$v^+ = \frac{v}{L \Omega_{eq}}$$

and the dimensionless Subcooling number [10,18]

$$N_s = \frac{i_{f,sat}^{-i_\lambda}}{\Delta i_{fg}} \frac{\Delta \rho}{\rho_{g,sat}} \quad (3.28)$$

Hence, the dimensionless form of equations (3.19) to (3.21) are

$$\frac{1}{\rho^+} \frac{D\rho^+}{Dt^+} = -\Gamma^+ \quad (3.29)$$

$$\frac{\partial v^+}{\partial z^+} = \Gamma^+ \quad (3.30)$$

$$\rho^+ \frac{Di^+}{Dt^+} = \frac{1}{N_s} \quad (3.31)$$

From equation (3.12) and using the boundary condition

$$\text{@ } i^+ = 0, \Gamma^+ = 0 \quad (3.32)$$

one obtains

$$i^+ = -\ln(1-\Gamma^+) \quad (3.33)$$

Substitution of (3.33) into (3.31) results in

$$N_s \rho^+ \frac{D \ln(1-\Gamma^+)}{Dt^+} = -1 \quad (3.34)$$

From (3.29)

$$\frac{1}{\rho^+ \Gamma^+} \frac{D \rho^+}{Dt^+} = -1 \quad (3.35)$$

Equating (3.34) and (3.35)

$$\frac{1}{\rho^{+2}} \frac{D \rho^+}{Dt^+} = N_s \Gamma^+ \frac{D \ln(1-\Gamma^+)}{Dt^+} \quad (3.36)$$

or

$$\frac{D(1/\rho^+)}{Dt^+} = N_s \frac{\Gamma^+}{1-\Gamma^+} \frac{D\Gamma^+}{Dt^+} \quad (3.37)$$

Hence, following the center of gravity of the mixture, equation (3.37) may be integrated from the point of net vapor formation, λ , where

$$\rho^+ = \frac{\rho}{\rho_{f,sat}} = 1, \Gamma^+ = 0$$

to some point downstream where

$$\rho^+ = \rho^+, \Gamma^+ = \Gamma^+$$

Therefore,

$$\int_1^{\rho^+} d\left(\frac{1}{\rho^+}\right) = N_s \int_0^{\Gamma^+} \frac{\Gamma^+}{1-\Gamma^+} d\Gamma^+ \quad (3.38)$$

or

$$\frac{1}{\rho^+} - 1 = N_s [1 - \Gamma^+ - \ln(1-\Gamma^+)] \Big|_0^{\Gamma^+} \quad (3.39)$$

or

$$\frac{1}{\rho^+} - 1 = N_s [-\Gamma^+ - \ln(1-\Gamma^+)] \quad (3.40)$$

whence is obtained the expression for the density of the mixture (valid for the homogeneous flow model)

$$\frac{1}{\rho^+} = 1 - N_s [\Gamma^+ + \ln(1-\Gamma^+)] \quad (3.41)$$

In order to obtain the true vapor quality it is noted that, in conjunction with equations (3.23) and (3.17), equation

(3.41) may be rewritten as

$$x \frac{\Delta p}{\rho_{g,sat}} = N_s \left[\ln \frac{1}{1-\Gamma^+} - \Gamma^+ \right] \quad (3.42)$$

or, in view of (3.33)

$$x \frac{\Delta p}{\rho_{g,sat}} = N_s [i^+ - (1-e^{-i^+})] \quad (3.43)$$

Substitution of (3.22) and (3.28) for the dimensionless quantities i^+ and N_s results in the following expression for the true vapor quality

$$x = \frac{i(z) - i_{f,sat}}{\Delta i_{fg}} + \frac{i_{f,sat}^{-i_\lambda}}{\Delta i_{fg}} \exp\left[-\frac{i(z) - i_\lambda}{i_{f,sat}^{-i_\lambda}}\right] \quad (3.44)$$

Now since

$$x_{eq} = \frac{i(z) - i_{f,sat}}{\Delta i_{fg}} \quad (3.45)$$

and

$$\frac{i_{f,sat}^{-i_\lambda}}{\Delta i_{fg}} = \frac{c_p \Delta T_{sub}}{\Delta i_{fg}} \quad (3.46)$$

and

$$i^+ = \frac{i(z) - i_\lambda}{i_{f,sat} - i_\lambda} = x_{eq} \frac{\Delta i_{fg}}{i_{f,sat} - i_\lambda} + 1 \quad (3.47)$$

the true vapor quality can be expressed also as

$$x = x_{eq} + \frac{c_p \Delta T_{sub}}{\Delta i_{fg}} \exp[-1 - x_{eq} \frac{\Delta i_{fg}}{c_p \Delta T_{sub}}] \quad (3.48)$$

It should be noted that this expression for the true vapor quality (which was obtained from the model presented in section 3.1) is identical to the expression which was postulated by Levy [13].

One additional point is made here. From equation (3.12)

$$\Gamma^+ = 1 - e^{-i^+}$$

which, in dimensional form becomes

$$\Gamma_g = \frac{q''_w \xi}{\Delta i_{fg} A} [1 - \exp\{-\frac{i(z) - i_\lambda}{i_{f,sat} - i_\lambda}\}] \quad (3.49)$$

Since, for steady state

$$\frac{i(z) - i_\lambda}{i_{f,sat} - i_\lambda} = \frac{z - \lambda}{\Delta \ell}$$

it can be seen that equation (3.49) reduces to the formulation of Saha [18], i.e. equation (2.15), for steady state flow.

CHAPTER IV

COMPARISON WITH EXPERIMENTS AND DISCUSSION

Since an expression for the true vapor quality is available, one can use the relationship presented in [12,23,3,18] to evaluate the vapor void fraction

$$\langle \alpha \rangle = \frac{x}{C_o \frac{\Delta \rho}{\rho_f} x + [C_o + \frac{\bar{V}_{gj}}{v_{fi}}] \frac{\rho_g}{\rho_f}} \quad (4.1)$$

where the weighted mean drift velocity for upward bubbly churn flow is calculated from

$$\bar{V}_{gj} = 1.41 \left[\frac{\sigma g \Delta \rho}{2 \rho_f} \right]^{1/4} \quad (4.2)$$

the distribution parameter, C_o , by

$$C_o = \frac{\langle \alpha_j \rangle}{\langle \alpha \rangle \langle j \rangle} \quad (4.3)$$

and the true vapor quality from equation (3.48). It was recommended in [12] that, in the absence of accurate

experimental data a value of $C_0 = 1.13$ for circular geometries be used in equation (4.1) for predicting the area average void fraction, α . That value will be used in the present work in order to predict the vapor void fraction.

The point in a duct where significant voids first appear is defined as the point of net vapor generation [18,19]. A new method for accurately predicting this point has been developed in [18,19], and will be used in the present work in order to establish a starting point for the axial void fraction distribution. The results are

$$x_\lambda = - \frac{c_p \Delta T_{\text{sub}}}{\Delta i_{\text{fg}}} = -0.0022 \frac{\dot{q}''_w}{\rho_{f,\text{sat}} \Delta i_{\text{fg}}} \frac{D_h}{a_f} \quad (4.4)$$

$$\text{if } Pe \leq 70,000$$

and

$$x = - \frac{c_p \Delta T_{\text{sub}}}{\Delta i_{\text{fg}}} = -154 \frac{\dot{q}''_w}{\rho_{f,\text{sat}} \Delta i_{\text{fg}}} \frac{1}{v_{fi}} \quad (4.5)$$

$$\text{if } Pe \geq 70,000$$

where the Peclet number is defined as

$$Pe = \frac{(G D_h c_{p_f})_{\text{sat}}}{k_{f,\text{sat}}} \quad (4.6)$$

Hence, the axial position of net vapor formation, z_λ , is

$$z_\lambda = - \frac{x_\lambda \Delta i_{fg}}{q''_w \xi} \quad (4.7)$$

The predicted results are compared with various experimental data in Figures 11 through 13. The data and predictions are plotted versus equilibrium quality, x_{eq} , in order to highlight the large errors which can result from using a strictly equilibrium approach toward predicting vapor void fraction. As can be seen from Figures 11 through 13, local vapor void fractions in excess of 30% have been measured in the region of subcooled boiling.

It is evident that the agreement between the theoretical prediction and the available experimental data is quite satisfactory. This seems to validate the present model and the constitutive equation of net vapor generation, Γ_g , postulated in this thesis.

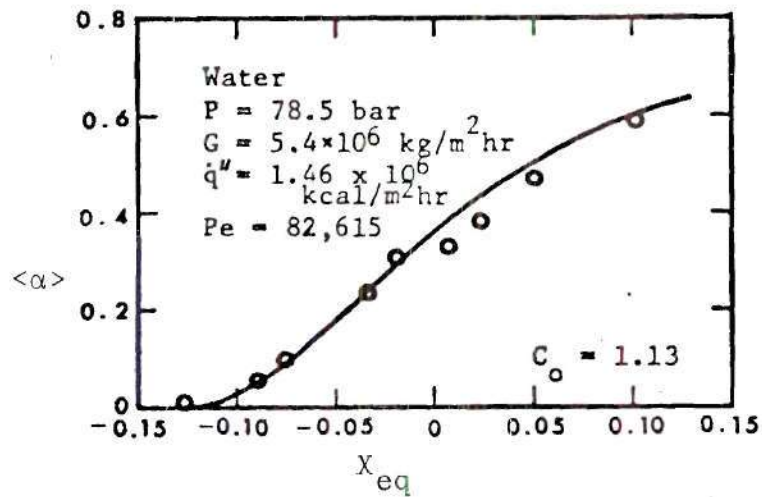


Figure 11. Comparison Between Predicted and Measured Vapor Void Fraction. Data of Martin [28].

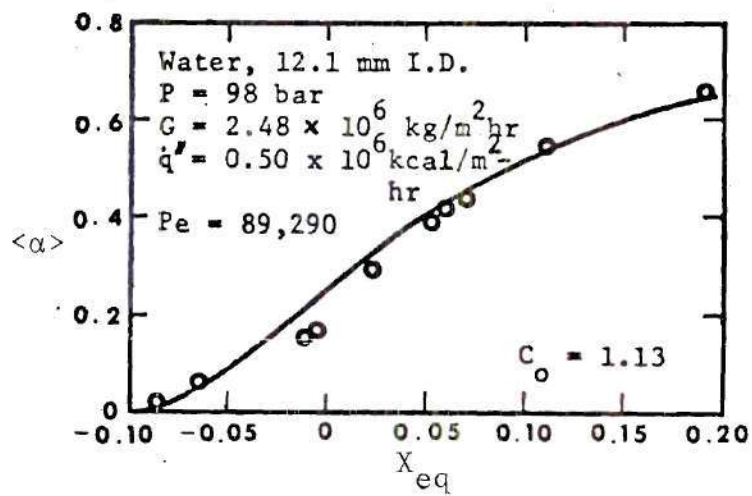


Figure 12. Comparison Between Predicted and Measured Vapor Void Fraction. Data of Lobachev, et al. [29].

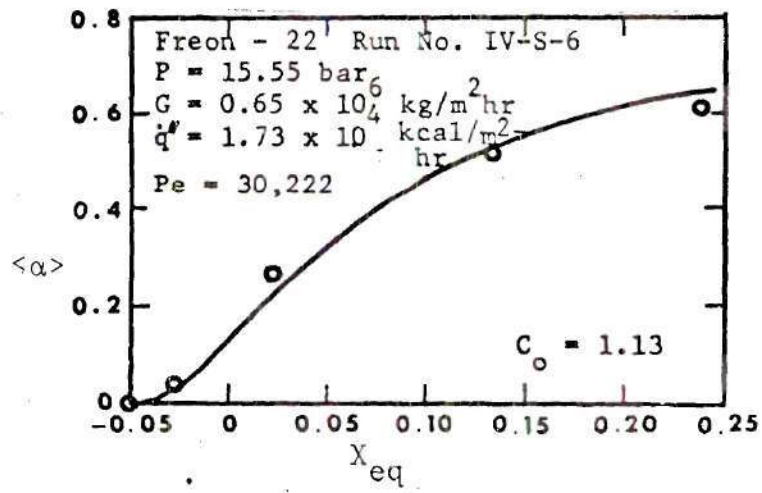


Figure 13. Comparison Between Predicted and Measured Vapor Void Fraction. Data of Staub, et al. [30].

CHAPTER V

CONCLUSIONS

The following conclusions can be drawn:

(1) the postulated constitutive equation of net evaporation is given by a first order rate equation, valid for both steady state and transient flow.

(2) using this constitutive equation in conjunction with the field equations for the homogeneous flow model, expressions for mixture density and true vapor quality were derived.

(3) good agreement is shown between predicted void fractions (based on the model) and experimental data for subcooled boiling.

APPENDICES

APPENDIX A

MARTINELLI-NELSON CORRELATION

Lockhart and Martinelli [14] have developed a procedure for calculating the frictional pressure gradient of an adiabatic two-phase flow of air and various liquids at atmospheric pressure.

For the prediction of pressure drop during forced convection boiling, Martinelli and Nelson [15] postulated that the flow regime would always be turbulent--turbulent for the purpose of extending the Lockhart-Martinelli data [14]. Their model is based upon the following assumptions:

- i) the validity of extending the Lockhart-Martinelli curves [14] of $\phi_{f_{tt}}$ versus χ_{tt} for flow of air and various liquids to boiling water.
- ii) the validity of a point to point evaluation of $\phi_{f_{tt}}$ and $(\frac{dp}{dz} F)_{fo}$ and their integration.
- iii) the validity of extrapolating curves of $\phi_{f_{tt}}$ and α to the critical point.
- iv) that the relationship between mass quality and length is linear (i.e. the assumption of thermodynamic equilibrium between phases).

From these assumptions, Martinelli and Nelson constructed their results as follows:

- i) the local value of ϕ_{fo}^2 was plotted versus local mass quality x_{eq} and various pressures as shown in Figure 14. The curves at pressures between the atmospheric and critical pressures were established by trial and error using the data of Davidson [6] as a guide.
- ii) The overall value of $\frac{1}{x_{eq}} \int_0^{x_{eq}} \phi_{fo}^2 dx_{eq}$ was evaluated graphically from Figure 14 and plotted versus exit quality and pressure as shown in Figure 15, by assuming that the relationship between x_{eq} and z is linear (corresponding to the case of uniform wall heat flux along with thermodynamic equilibrium).

The frictional component of pressure drop is thus evaluated from the Martinelli-Nelson correlation. From the expression for the separated flow model

$$-(\Delta p)_{fric} = \frac{f_{fo} G^2 z_e}{2 \rho_f D_h} \frac{1}{x_{eq}} \int_0^{x_{eq}} \phi_{fo}^2 dx_{eq} \quad (1.8)$$

where the value of $\frac{1}{x_{eq}} \int_0^{x_{eq}} \phi_{fo}^2 dx_{eq}$ is obtained from Figure 15 at the value of reduced pressure $\frac{p}{p_c}$, for the data being evaluated.

Prediction of void fraction is likewise required in order to evaluate both the acceleration and gravitational pressure drop from the separated flow model. Martinelli and

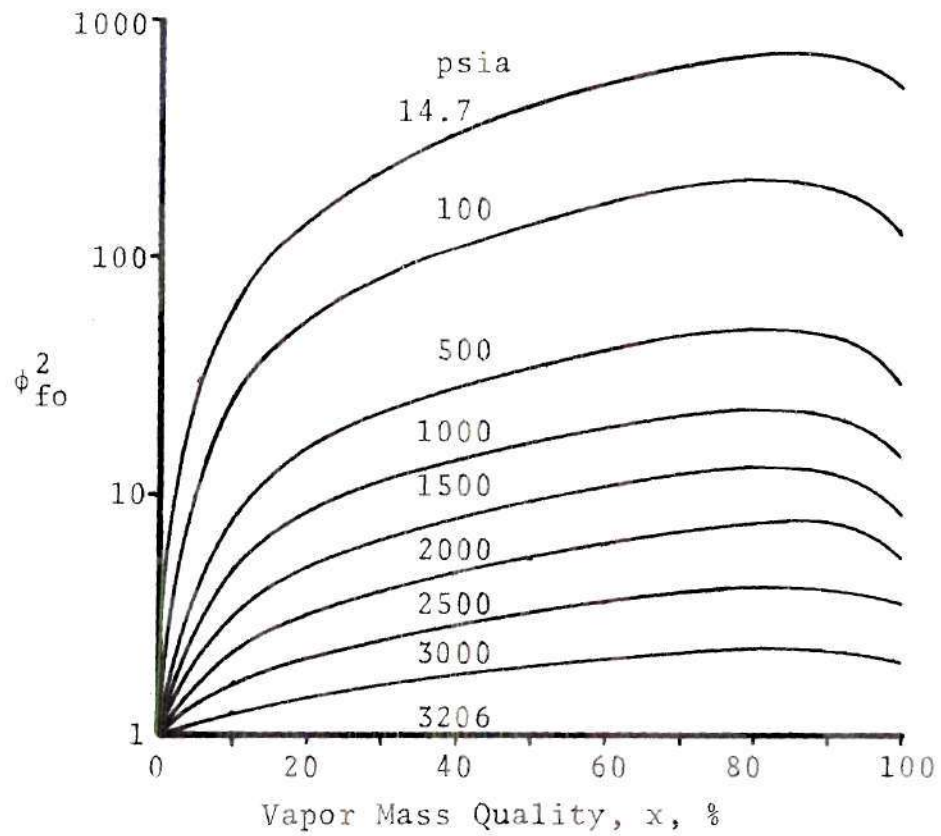


Figure 14. Ratio of Local Two-Phase Pressure Gradient to Pressure Gradient for 100% Liquid Flow as a Function of Quality and Pressure, Steam-Water (Martinelli-Nelson)

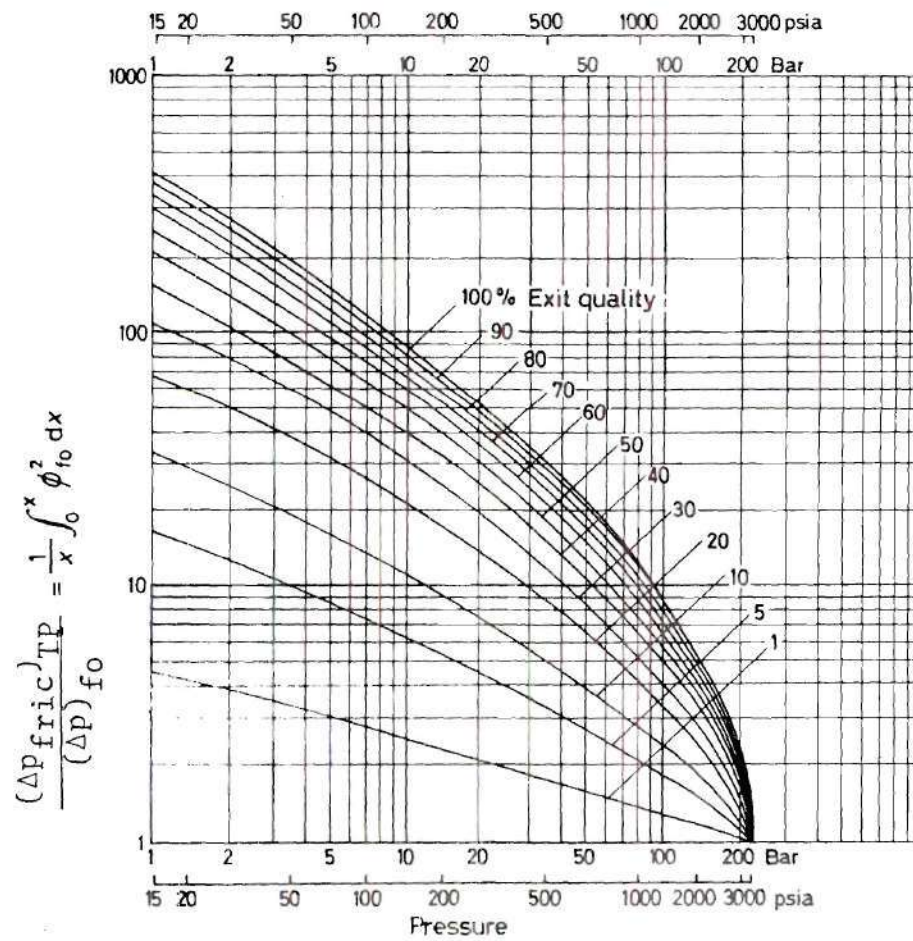


Figure 15. Ratio, $\frac{(\Delta p_{\text{fric}})_{\text{TP}}}{(\Delta p)_{\text{fo}}}$ as a Function of Exit Quality and Pressure, Steam-Water (Martinelli-Nelson)

Nelson utilized the Lockhart-Martinelli correlation for void fraction, and constructed curves of void fraction versus equilibrium mass quality and pressure in the same manner as for the frictional correlation. Their results are shown in Figure 16.

In order to ease computation of the separated flow model acceleration pressure drop,

$$-(\Delta p)_{\text{accel}} = \frac{G^2}{\rho_f} \left[\frac{x_{\text{eq}}^2}{\alpha} \left(\frac{\rho_f}{\rho_g} \right) + \frac{(1-x_{\text{eq}})^2}{1-\alpha} - 1 \right] \quad (1.9)$$

values of the bracketed term in equation (1.9), designated r_2 , have been evaluated using the values of void fraction in Figure 16. These values are shown in Figure 17 as a function of pressure with exit equilibrium mass quality as a parameter. As with the frictional term, the Martinelli-Nelson curve is entered at the value of reduced pressure for the data being evaluated.

Finally, in order to evaluate the gravitational pressure drop,

$$-(\Delta p)_g = \frac{g \rho_f z_e \sin \theta}{x_{\text{eq}}} \int_0^{x_{\text{eq}}} \left[(1-\alpha) + \frac{\rho_g}{\rho_f} \alpha \right] dx_{\text{eq}} \quad (1.10)$$

it is necessary to use the void fraction correlation presented above. In the present thesis, the above integral

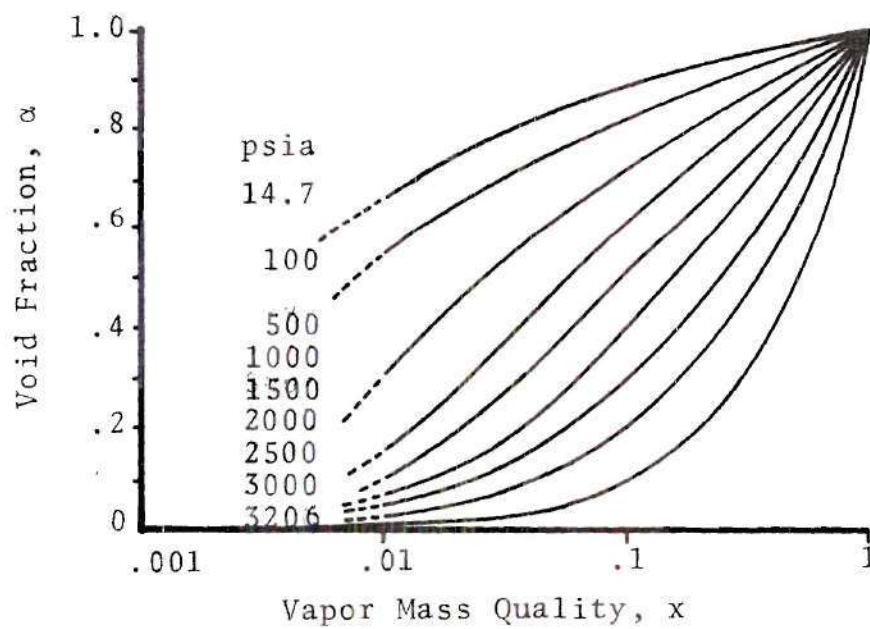


Figure 16. Void Fraction, α , as a Function of Quality and Absolute Pressure, Steam-Water (Martinelli-Nelson)

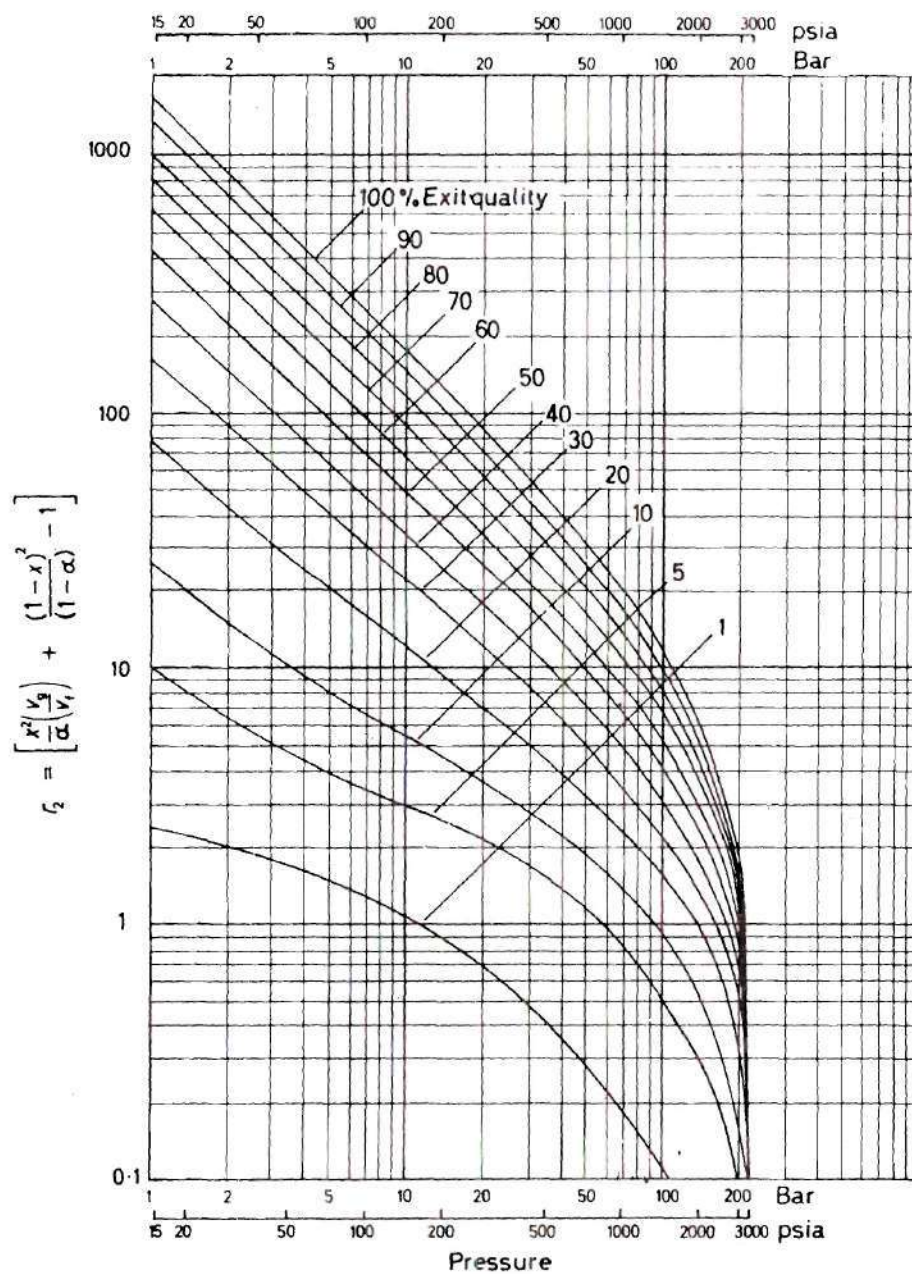


Figure 17. Multiplier, r_2 , as a Function of Pressure for Various Exit Qualities, Steam-Water (Martinelli-Nelson)

was determined graphically, where the integrand of equation (1.10) was evaluated by use of Figure 16.

Baroczy Correlation

Experimental data subsequent to the development of the Martinelli-Nelson correlation have indicated that the values of ϕ_{fo}^2 are mass-velocity dependent [9]. Data which show this effect are given on Figure 18 [9]. Recent attempts to correct existing models for the influence of mass velocity on the friction multiplier, ϕ_{fo}^2 , include one proposed by Baroczy [2].

In his method, Baroczy employs two sets of curves which were derived from wide ranging experimental data (mass flux, fluid properties, heat flux, mass quality). The first is a plot of the two-phase frictional multiplier ϕ_{fo}^2 versus a fluid physical property index $\left(\frac{\mu_f}{\mu_g}\right)^{0.2} \frac{\rho_g}{\rho_f}$ with mass quality as a parameter for a reference mass velocity of 10^6 lbm/hr-ft² (Figure 19). The second is a plot of correction factor, Ω , expressed as a function of the same physical property index for mass velocities of .25, .50, 2.0, and 3.0×10^6 lbm/hr-ft² with mass quality as a parameter (Figure 20). The purpose of the second plot is to correct the value of ϕ_{fo}^2 obtained from Figure 19 to the appropriate value of mass flux. Baroczy attributes the whimsical fluctuations in the curves of Figure 19 as representing changing flow patterns. Thus

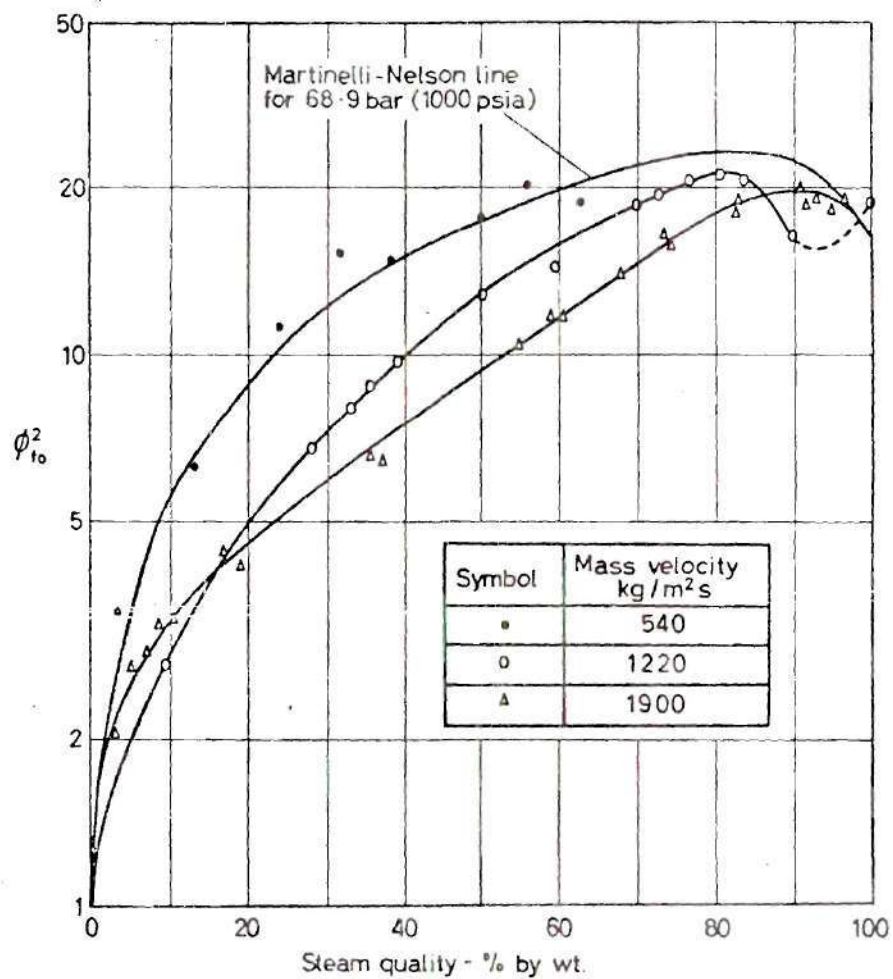


Figure 18. Effect of Mass Velocity on the Value of ϕ_{fo}^2 at a Pressure of 68.9 Bar

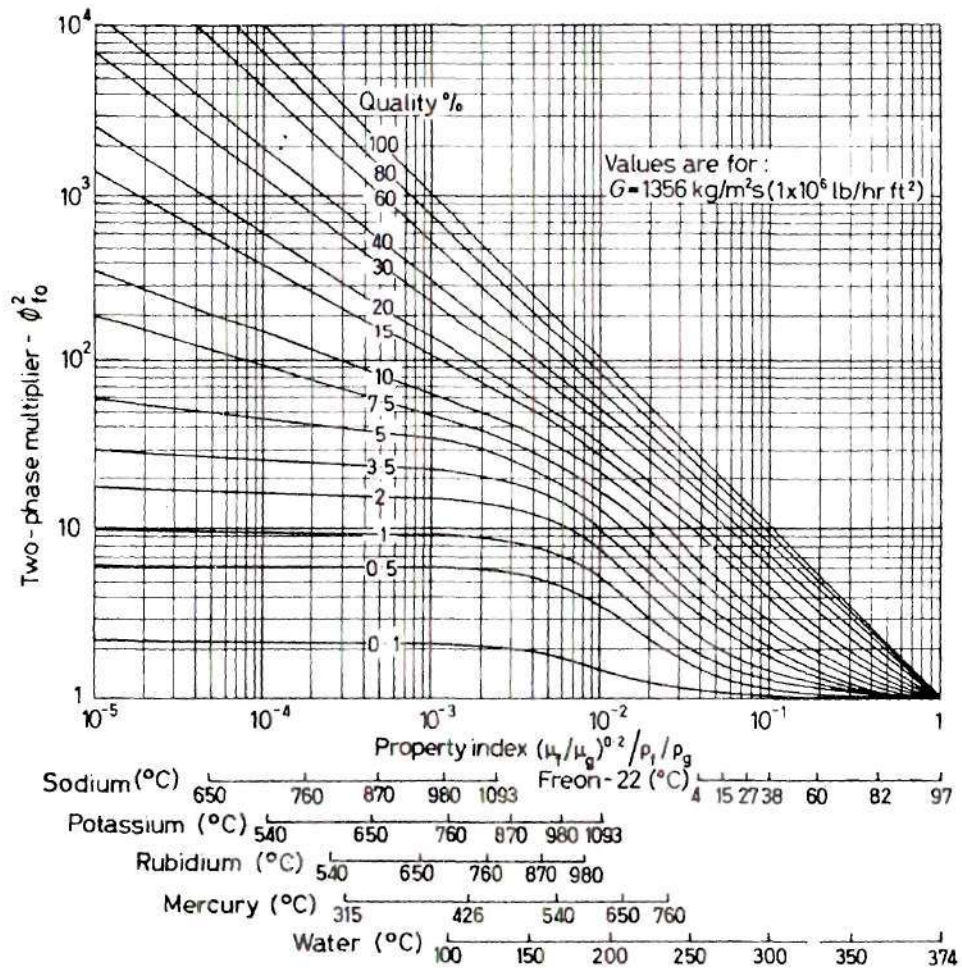


Figure 19. Two-Phase Frictional Pressure Drop Correlation (Baroczy)

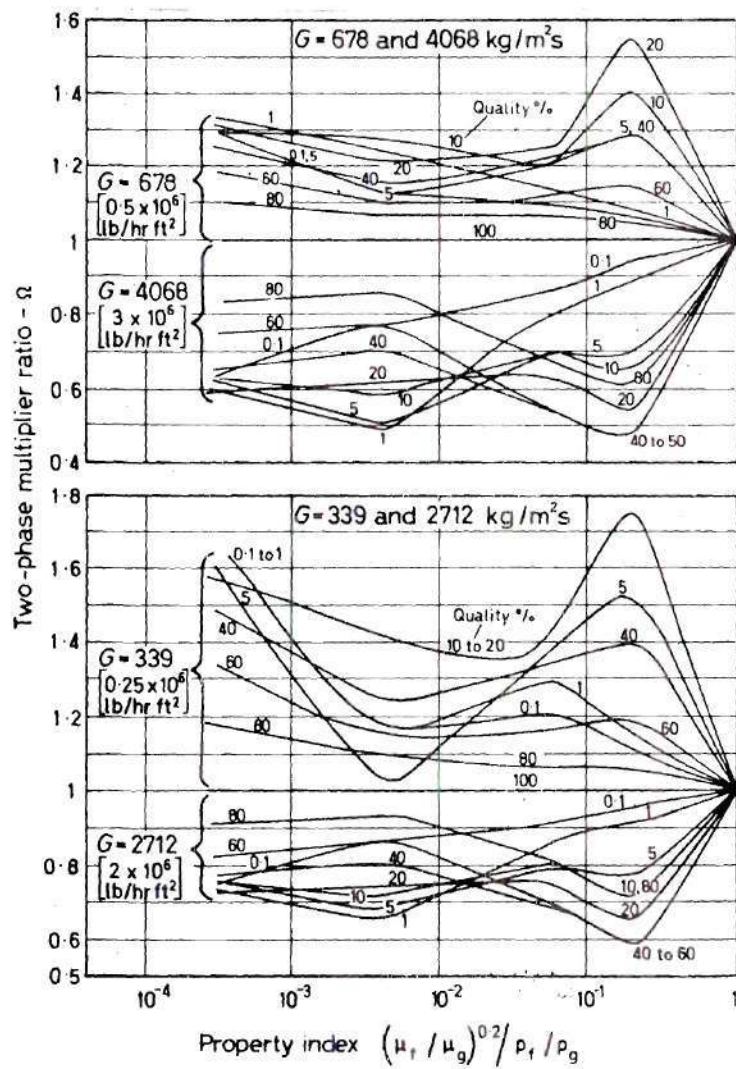


Figure 20. Mass Velocity Correction Versus Property Index (Baroczy)

$$-\left(\frac{dp}{dz}\right)_{\text{fric}} = \frac{f_{fo} G^2}{2\rho_f D_h} \phi_{fo}^2 (G = 10^6 \text{ lbm/hr-ft}^2)^{\Omega} \quad (\text{A.1})$$

Hence

$$-(\Delta p)_{\text{fric}} = \frac{f_{fo} G^2 z_e}{2\rho_f D_h (x_{eq})_e} \int_0^{x_{eq}} \phi_{fo}^2 (G = 10^6)^{\Omega} dx_{eq} \quad (\text{A.2})$$

where

$$dz = dz \frac{dx_{eq}}{dz} \frac{dz}{dx_{eq}} = \frac{z_e}{(x_{eq})_e} dx_{eq}$$

since

$$\frac{dz}{dx_{eq}} = \frac{z_e}{(x_{eq})_e}$$

for the thermodynamic equilibrium model.

The integral of equation (A.2) was determined graphically by constructing a curve of $\phi_{fo}^2 (G=10^6)^{\Omega}$ versus equilibrium quality, x_{eq} . The frictional pressure drop as estimated by the Baroczy method was thereby determined. In accordance with current practice [4], the gravitational and accelerational pressure drops are calculated from the Martinelli-Nelson method. The results are exhibited in Tables 1 through 28.

Prediction of Vapor Void Fraction

As shown in [12,23] the average void fraction can be expressed in general as

$$\langle \alpha \rangle = \frac{x}{C_0 \left[\frac{x \Delta \rho}{\rho_f} + \frac{\rho_g}{\rho_f} \right] + \frac{\rho_g V g j}{G}} \quad (\text{A.3})$$

where C_0 is the distribution parameter which corrects the one-dimensional homogeneous theory to account for the fact that concentration and velocity profiles across the channel can vary independently of one another. A value of $C_0 = 1.13$ has correlated well with previous data without reference to the flow pattern, and was used in the present evaluation.

The mass quality, x , in equation (A.3) is the true vapor quality. This was obtained in [12,23] from the postulation of a dimensionless enthalpy distribution to account for thermal non-equilibrium

$$i_f^+ = \frac{i_f(z) - i_{f\lambda}}{i_{f,sat} - i_{f\lambda}} = 1 - \exp\left\{-\frac{i(z) - i_{f\lambda}}{i_{f,sat} - i_{f\lambda}}\right\} \quad (\text{A.4})$$

where $i_{f,sat}$ and $i_{f\lambda}$ are the liquid enthalpies at saturation and at the point of initial vapor formation respectively.

By using the standard definition of true mass quality

$$x = \frac{i(z) - i_f(z)}{i_g(z) - i_f(z)} \quad (\text{A.5})$$

and of equilibrium quality

$$x_{eq} = \frac{i(z) - i_{f,sat}}{\Delta i_{fg}} \quad (\text{A.6})$$

equation (A.4) becomes

$$1 + \frac{\Delta i_{fg}}{c_p \Delta T_{sub}} \frac{(x - x_{eq})}{1 - x} = 1 - \exp\left\{-\frac{x_{eq} \Delta i_{fg}}{c_p \Delta T_{sub}} - 1\right\} \quad (\text{A.7})$$

whence

$$x = \frac{x_{eq} + \frac{c_p \Delta T_{sub}}{\Delta i_{fg}} \exp\left\{-\frac{x_{eq} \Delta i_{fg}}{c_p \Delta T_{sub}} - 1\right\}}{1 + \frac{c_p \Delta T_{sub}}{\Delta i_{fg}} \exp\left\{-\frac{x_{eq} \Delta i_{fg}}{c_p \Delta T_{sub}} - 1\right\}} \quad (\text{A.8})$$

In order to close the problem, it is necessary to predict z_λ , the point of net vapor generation.

In his Ph.D. thesis, Saha [18] has developed a general correlation which can predict accurately the point of net vapor generation for all mass flow rates. His results are

$$x_\lambda = - \frac{c_p \Delta T_{\text{sub}}}{\Delta i_{fg}} = -0.0022 \frac{\dot{q}''_w}{\rho_f \Delta i_{fg}} \frac{D_h}{a_f} \text{ if } P_e \leq 70,000 \quad (\text{A.9})$$

$$= -154 \frac{\dot{q}''_w}{\rho_f \Delta i_{fg}} \frac{1}{v_{f,i}} \text{ if } P_e \geq 70,000 \quad (\text{A.10})$$

where the Peclet number is

$$P_e = \frac{G D_h c_{p_f}}{k_f} \quad (\text{A.11})$$

and all fluid properties are saturation values. From equations (A.9) and (A.10) the axial position for the point of net vapor formation can be determined as follows

$$z_\lambda = - \frac{x_\lambda W \Delta i_{fg}}{\dot{q}''_w \xi} \quad (\text{A.12})$$

The above non-equilibrium formulations were utilized in conjunction with the Armand-Lottes-Levy model of the mixture friction factor (to follow), to integrate the mixture field equation (1.12).

Mixture Friction Factor

If one considers the entire liquid flow to be confined in a film with a smooth interface, and if one neglects gravitational and accelerational forces, a force balance on the combined phases, and then on the vapor phase yields [4]

$$\phi_f^2 = \frac{1}{(1-\alpha)^2} \quad (\text{A.13})$$

This expression reduces to

$$f_m = f_f \frac{\rho_m}{\rho_f} \left(\frac{1-x}{1-\alpha}\right)^2 \quad (\text{A.14})$$

where f_f is the single phase friction factor assuming the liquid phase alone to be flowing in the channel.

From the assumptions used in deriving (A.14), it can be seen that the model is applicable only to steady, isothermal, axisymmetric, horizontal flow, with a planar interface between phases. However, the expression is often utilized in practical applications.

Integration of Mixture Model Terms

As pointed out in 1.2.3, certain terms in the simplified mixture momentum equation are integrable only after one specifies the equations for void fraction and mixture friction factor. Hence,

$$-\Delta p_{\text{grav}} = \int_0^{z_e} g \rho_m dz = g \int_0^{z_e} \{\rho_f(1-\alpha) + \rho_g \alpha\} dz$$

$$-\Delta p_{\text{fric}} = \int_0^{z_e} \frac{f_m}{2D_h} \rho_m v_m^2 dz = \frac{f_f G^2}{2\rho_f D_h} \int_0^{z_e} \left(\frac{1-x}{1-\alpha}\right)^2 dz$$

where the various terms have been previously defined. The equation for void fraction, α , has been given by (A.3), and that for true vapor quality, x , by equation (A.8). The length of two-phase flow in the channel according to this non-equilibrium model is determined according to

$$z_e = (L - z_{eq}) + z_\lambda$$

where z_λ is given by equation (A.12). Hence, the non-equilibrium model length for two-phase flow is the sum of the equilibrium length and the difference in the length between the point of net vapor generation for non-equilibrium and equilibrium flow.

APPENDIX B

RESULTS OF PREDICTIVE METHODS AND EXPERIMENTAL DATA

Table 1. Results of Predictive Methods and Experimental Data

System pressure = 150 psia Inlet temperature = 243.5°F
 Mass flux = 1200809 lb_m/hr-ft² Inlet Reynolds number = 63780
 Heat flux (wall) = 12273 Btu/hr-ft² Room temperature = 74°F

Model	Predictive Methods					
	Viscosity x 10 ³ lb _m /ft-sec		ΔP _a psi	ΔP _g psi	ΔP _f psi	Total ΔP psi
Homogeneous	.1475	(1)	.031	.119	.021	.171
	.1483	(2)			.022	.171
	.1491	(3)			.022	.171
	.1521	(4)			.022	.171
Martinelli-Nelson			.031	.118	.028	.177
Baroczy			.031	.118	.026	.175
Armand-Lottes-Levy Equilibrium model:			.025	.120	.023	.167
Non-equil. model:			.065	.762	.156	.983

Experimental Pressure Drop			
Axial Coordinate feet	psi	P _i - P _{i-1} chart divisions	Total ΔP psi
1			
2	-.673	-1.0	-.673
3	-.673	-1.0	-1.346
4	-.676	-0.5	-2.022
5	-.666	-2.0	-2.688
6	-.684	0.5	-3.372
7	-.695	2.0	-4.067
8	-.691	1.5	-4.758
9	-.673	-1.0	-5.431
	Equilibrium Model	Non-Equilibrium Model	
Axial position of net vapor formation:	8.77 ft.	7.48 ft.	
Exit mass quality:	.0061	.0163	
Two-phase pressure drop:	-.156 psi	-1.032 psi	

Table 2. Results of Predictive Methods and Experimental Data

System pressure = 150 psia Inlet temperature = 243.5°F
 Mass flux = 1200809 lb_m/hr-ft² Inlet Reynolds number = 63780
 Heat flux (wall) = 14125 Btu/hr-ft² Room temperature = 74°F

Predictive Methods						
Model	Viscosity x 10 ³ lb _m /ft-sec		ΔP _a psi	ΔP _g psi	ΔP _f psi	Total ΔP psi
Homogeneous	.1475	(1)	.210	.567	.163	.940
	.1528	(2)			.164	.941
	.1590	(3)			.165	.942
	.1788	(4)			.167	.944
Martinelli-Nelson			.242	.552	.259	1.053
Baroczy			.242	.552	.252	1.046
Armand-Lottes-Levy Equilibrium model:			.161	.596	.197	.953
Non-equil. model:			.177	1.198	.357	1.733

Experimental Pressure Drop			
Axial Coordinate feet	psi	P _i - P _{i-1} chart divisions	Total ΔP psi
1			
2	-.669	-1.5	-.669
3	-.673	-1.0	-1.342
4	-.669	-1.5	-2.011
5	-.713	4.5	-2.724
6	-.647	-4.5	-3.371
7	-.702	3.0	-4.073
8	-.684	0.5	-4.757
9	-.651	-4.0	-5.408
	Equilibrium Model	Non-Equilibrium Model	
Axial position of net vapor formation:	7.62 ft.	6.33 ft.	
Exit mass quality:	.0418	.0465	
Two-phase pressure drop:	-.912 psi	-1.805 psi	

Table 3. Results of Predictive Methods
and Experimental Data

System pressure = 150 psia Inlet temperature = 243.5°F
 Mass flux = 1200809 lb_m/hr-ft² Inlet Reynolds number = 63780
 Heat flux (wall) = 15838 Btu/hr-ft² Room temperature = 74°F

Predictive Methods						
Model	Viscosity x 10 ³ lb _m /ft-sec		ΔP _a psi	ΔP _g psi	ΔP _f psi	Total ΔP psi
Homogeneous	.1475	(1)	.376	.777	.313	1.465
	.1573	(2)			.315	1.467
	.1688	(3)			.318	1.470
	.2034	(4)			.326	1.478
Martinelli-Nelson			.360	.764	.535	1.659
Baroczy			.360	.764	.545	1.669
Armand-Lottes-Levy Equilibrium model:			.273	.840	.421	1.534
Non-equil. model:			.282	1.429	.596	2.307

Experimental Pressure Drop				
Axial Coordinate feet	psi	P _i - P _{i-1} chart divisions	Total ΔP psi	
1				
2	-.676	-0.5		-.676
3	-.673	-1.0		-1.349
4	-.673	-1.0		-2.022
5	-.673	-1.0		-2.695
6	-.695	2.0		-3.390
7	-.687	1.0		-4.077
8	-.680	0		-4.757
9	-.680	0		-5.437
		Equilibrium Model	Non-Equilibrium Model	
Axial position of net vapor formation:		6.79 ft.	5.51 ft.	
Exit mass quality:		.0748	.0775	
Two-phase pressure drop:		-1.502 psi	-2.391 psi	

Table 4. Results of Predictive Methods and Experimental Data

System pressure = 150 psia Inlet temperature = 243.5°F
 Mass flux = 1200809 lb_m/hr-ft² Inlet Reynolds number = 63780
 Heat flux (wall) = 18274 Btu/hr-ft² Room temperature = 74°F

Predictive Methods						
Model	Viscosity x 10 ³ lb _m /ft-sec		ΔP _a psi	ΔP _g psi	ΔP _f psi	Total ΔP psi
Homogeneous	.1475	(1)	.611	.924	.545	2.080
	.1642	(2)			.553	2.088
	.1837	(3)			.561	2.096
	.2385	(4)			.580	2.115
Martinelli-Nelson			.521	.931	.994	2.446
Baroczy			.521	.931	1.055	2.507
Armand-Lottes-Levy Equilibrium model:			.414	1.034	.818	2.267
Non-equil. model:			.419	1.611	1.008	3.038

Experimental Pressure Drop			
Axial Coordinate feet	psi	P _i - P _{i-1} chart divisions	Total ΔP psi
1			
2	-.673	-1.0	-.673
3	-.680	0	-1.353
4	-.673	-1.0	-2.026
5	-.680	0	-2.706
6	-.680	0	-3.386
7	-.695	2.0	-4.081
8	-.702	3.0	-4.783
9	-.695	2.0	-5.478
	Equilibrium Model	Non-Equilibrium Model	
Axial position of net vapor formation:	5.89 ft.	4.6 ft.	
Exit mass quality:	.1217	.1232	
Two-phase pressure drop:	-2.167 psi	-3.043 psi	

Table 5. Results of Predictive Methods and Experimental Data

System pressure = 150 psia Inlet temperature = 243.5°F
 Mass flux = 1200809 lb_m/hr-ft² Inlet Reynolds number = 63780
 Heat flux (wall) = 20762 Btu/hr-ft² Room temperature = 74°F

Predictive Methods					
Model	Viscosity x 10 ³ lb _m /ft-sec	ΔP_a psi	ΔP_g psi	ΔP_f psi	Total ΔP psi
Homogeneous	.1475 (1)	.852	.986	.800	2.638
	.1719 (2)			.815	2.654
	.2003 (3)			.832	2.670
	.2744 (4)			.867	2.705
Martinelli-Nelson		.685	1.021	1.512	3.218
Baroczy		.685	1.021	1.653	3.359
Armand-Lottes-Levy Equilibrium model:		.541	1.138	1.288	2.968
Non-equil. model:		.543	1.705	1.490	3.740

Experimental Pressure Drop			
Axial Coordinate feet	psi	$P_i - P_{i-1}$ chart divisions	Total ΔP psi
1			
2	-.673	-1.0	-.673
3	-.676	-0.5	-1.349
4	-.680	0	-2.029
5	-.673	-1.0	-2.702
6	-.684	0.5	-3.386
7	-.720	5.5	-4.106
8	-.731	7.0	-4.837
9	-.745	9.0	-5.582
	Equilibrium Model	Non-Equilibrium Model	
Axial position of net vapor formation:	5.18 ft.	3.89 ft.	
Exit mass quality:	.1697	.1706	
Two-phase pressure drop:	-2.755 psi	-3.625 psi	

Table 6. Results of Predictive Methods and Experimental Data

System pressure = 175 psia Inlet temperature = 265°F
 Mass flux = 1168362 lb_m/hr-ft² Inlet Reynolds number = 67740
 Heat flux (wall) = 10161 Btu/hr-ft² Room temperature = 80°F

Predictive Methods						
Model	Viscosity x 10 ³ lb _m /ft-sec		ΔP _a psi	ΔP _g psi	ΔP _f psi	Total ΔP psi
Homogeneous	.1370	(1)	.040	.211	.039	.290
	.1382	(2)			.039	.291
	.1396	(3)			.039	.291
	.1448	(4)			.039	.291
Martinelli-Nelson			.049	.21	.05	.308
Baroczy			.049	.21	.047	.305
Armand-Lottes-Levy Equilibrium model:			.033	.214	.041	.287
Non-equil. model:			.057	.845	.167	1.069

Experimental Pressure Drop			
Axial Coordinate feet	psi	P _i - P _{i-1} chart divisions	Total ΔP psi
1			
2	-.651	-3.5	-.651
3	-.640	-5.0	-1.291
4	-.655	-3.0	-1.946
5	-.648	-4.0	-2.594
6	-.669	-1.0	-3.263
7	-.677	0	-3.940
8	-.677	0	-4.617
9	-.611	-9.0	-5.778
	Equilibrium Model	Non-Equilibrium Model	
Axial position of net vapor formation:	8.57 ft.	7.28 ft.	
Exit mass quality:	.0101	.0179	
Two-phase pressure drop:	-.263 psi	-1.097 psi	

Table 7. Results of Predictive Methods and Experimental Data

System pressure = 175 psia Inlet temperature = 265°F
 Mass flux = 1168362 lb_m/hr-ft² Inlet Reynolds number = 67740
 Heat flux (wall) = 11945 Btu/hr-ft² Room temperature = 80°F

Predictive Methods					
Model	Viscosity x 10 ³ lb _m /ft-sec	ΔP_a psi	ΔP_g psi	ΔP_f psi	Total ΔP psi
Homogeneous	.1370 (1)	.189	.696	.190	1.074
	.1427 (2)			.191	1.075
	.1498 (3)			.192	1.077
	.1736 (4)			.196	1.080
Martinelli-Nelson		.208	.678	.296	1.182
Baroczy		.208	.678	.285	1.171
Armand-Lottes-Levy Equilibrium model:		.145	.728	.227	1.100
Non-equil. model:		.155	1.330	.371	1.856

Experimental Pressure Drop			
Axial Coordinate feet	psi	$P_i - P_{i-1}$ chart divisions	Total ΔP psi
1			
2	-.651	-3.5	-.651
3	-.637	-5.5	-1.288
4	-.655	-3.0	-1.945
5	-.655	-3.0	-2.598
6	-.669	-1.0	-3.267
7	-.669	-1.0	-3.936
8	-.648	-4.0	-4.584
9	-.590	-12.0	-5.174

	Equilibrium Model	Non-Equilibrium Model
Axial position of net vapor formation:	7.29 ft.	6.00 ft.
Exit mass quality:	.0471	.0504
Two-phase pressure drop:	-1.049 psi	-1.905 psi

Table 8. Results of Predictive Methods and Experimental Data

System pressure = 175 psia Inlet temperature = 265°F
 Mass flux = 1168362 lb_m/hr-ft² Inlet Reynolds number = 67740
 Heat flux (wall) = 13873 Btu/hr-ft² Room temperature = 80°F

Predictive Methods						
Model	Viscosity x 10 ³ lb _m /ft-sec		ΔP _a psi	ΔP _g psi	ΔP _f psi	Total ΔP psi
Homogeneous	.1370	(1)	.349	.948	.364	1.661
	.1480	(2)			.368	1.664
	.1616	(3)			.372	1.668
	.2048	(4)			.383	1.680
Martinelli-Nelson			.319	.933	.611	1.863
Baroczy			.319	.933	.625	1.877
Armand-Lottes-Levy Equilibrium model:			.255	1.022	.485	1.761
Non-equil. model:			.259	1.611	.640	2.510

Experimental Pressure Drop			
Axial Coordinate feet	psi	P _i - P _{i-1} chart divisions	Total ΔP psi
1			
2	-.655	-3.0	-.655
3	-.640	-5.0	-1.295
4	-.662	-2.0	-1.957
5	-.655	-3.0	-2.612
6	-.666	-1.5	-3.278
7	-.655	-3.0	-3.933
8	-.633	-6.0	-4.566
9	-.615	-8.5	-5.181
	Equilibrium Model	Non-Equilibrium Model	
Axial position of net vapor formation:	6.28 ft.	4.99 ft.	
Exit mass quality:	.0871	.0888	
Two-phase pressure drop:	-1.721 psi	-2.576 psi	

Table 9. Results of Predictive Methods
and Experimental Data

System pressure = 175 psia Inlet temperature = 265°F
 Mass flux = 1168362 lb_m/hr-ft² Inlet Reynolds number = 67740
 Heat flux (wall) = 15945 Btu/hr-ft² Room temperature = 80°F

Predictive Methods						
Model	Viscosity x 10 ³ lb _m /ft-sec		ΔP _a psi	ΔP _g psi	ΔP _f psi	Total ΔP psi
Homogeneous	.1370	(1)	.521	1.076	.559	2.157
	.1540	(2)			.567	2.165
	.1754	(3)			.577	2.174
	.2383	(4)			.600	2.198
Martinelli-Nelson			.439	1.086	.979	2.505
Baroczy			.439	1.086	1.05	2.531
Armand-Lottes-Levy Equilibrium model:			.361	1.192	.810	2.364
Non-equil. model:			.363	1.772	.975	3.111

Experimental Pressure Drop			
Axial Coordinate feet	psi	P _i - P _{i-1} chart divisions	Total ΔP psi
1			
2	-.659	-2.5	-.659
3	-.644	-4.5	-1.303
4	-.662	-2.0	-1.965
5	-.655	-3.0	-2.620
6	-.662	-2.0	-3.782
7	-.640	-5.0	-3.922
8	-.648	-4.0	-4.570
9	-.626	-7.0	-5.196

	Equilibrium Model	Non-Equilibrium Model
Axial position of net vapor formation:	5.46 ft.	4.17 ft.
Exit mass quality:	.1301	.1311
Two-phase pressure drop:	-2.270 psi	-3.118 psi

Table 10. Results of Predictive Methods
and Experimental Data

System pressure = 175 psia Inlet temperature = 266°F
 Mass flux = 1987725 lb_m/hr-ft² Inlet Reynolds number = 115606
 Heat flux (wall) = 20452 Btu/hr-ft² Room temperature = 73°F

Predictive Methods						
Model	Viscosity x 10 ³ lb _m /ft-sec		ΔP _a psi	ΔP _g psi	ΔP _f psi	Total ΔP psi
Homogeneous	.1370	(1)	.643	.785	.587	2.016
	.1438	(2)			.591	2.019
	.1522	(3)			.595	2.024
	.1802	(4)			.608	2.037
Martinelli-Nelson			.679	.765	.936	2.38
Baroczy			.679	.765	.780	2.224
Armand-Lottes-Levy Equilibrium model:			.504	.823	.728	2.054
Non-equil. model:			.526	1.421	1.104	3.050

Experimental Pressure Drop				
Axial Coordinate feet	psi	P _i - P _{i-1} chart divisions		Total ΔP psi
1				
2	-.753	10.0		-.753
3	-.735	7.5		-1.488
4	-.750	9.5		-2.238
5	-.782	14.0		-3.020
6	-.826	20.0		-3.846
7	-.913	32.0		-4.759
8	-.876	27.0		-5.635
9	-.818	29.0		-6.453
		Equilibrium Model	Non-Equilibrium Model	
Axial position of net vapor formation:	7.00 ft.		5.71 ft.	
Exit mass quality:	.0555		.0581	
Two-phase pressure drop:	-1.695 psi		-2.846 psi	

Table 11. Results of Predictive Methods
and Experimental Data

System pressure = 175 psia Inlet temperature = 266°F
 Mass flux = 1987725 lb_m/hr-ft² Inlet Reynolds number = 115606
 Heat flux (wall) = 22953 Btu/hr-ft² Room temperature = 73°F

Predictive Methods						
Model	Viscosity x 10 ³ lb _m /ft-sec		ΔP _a psi	ΔP _g psi	ΔP _f psi	Total ΔP psi
Homogeneous	.1370	(1)	.997	.965	.932	2.894
	.1478	(2)			.941	2.903
	.1613	(3)			.951	2.914
	.2039	(4)			.981	2.943
Martinelli-Nelson			.915	.951	1.565	3.431
Baroczy			.915	.951	1.338	3.204
Armand-Lottes-Levy Equilibrium model:			.749	1.033	1.262	3.044
Non-equil. model:			.762	1.622	1.658	4.041

Experimental Pressure Drop				
Axial Coordinate feet	psi	P _i - P _{i-1} chart divisions		Total ΔP psi
1				
2	-.746	9.0		-.746
3	-.768	8.0		-1.514
4	-.746	9.0		-2.260
5	-.797	16.0		-3.057
6	-.866	25.5		-3.923
7	-.924	33.5		-4.847
8	-.873	26.5		-5.720
9	-.818	19.0		-6.538

	Equilibrium Model	Non-Equilibrium Model
Axial position of net vapor formation:	6.24 ft.	4.95 ft.
Exit mass quality:	.0860	.0876
Two-phase pressure drop:	-2.396 psi	-3.521 psi

Table 12. Results of Predictive Methods and Experimental Data

System pressure = 175 psia Inlet temperature = 266°F
 Mass flux = 1987725 lb_m/hr-ft² Inlet Reynolds number = 115606
 Heat flux (wall) = 25598 Btu/hr-ft² Room temperature = 73°F

Predictive Methods						
Model	Viscosity x 10 ³ lb _m /ft-sec		ΔP _a psi	ΔP _g psi	ΔP _f psi	Total ΔP psi
Homogeneous	.1370	(1)	1.371	1.073	1.306	3.750
	.1523	(2)			1.324	3.768
	.1715	(3)			1.344	3.788
	.2290	(4)			1.396	3.840
Martinelli-Nelson			1.176	1.071	2.274	4.521
Baroczy			1.176	1.071	1.989	4.236
Armand-Lottes-Levy Equilibrium model:			.989	1.170	1.900	4.060
Non-equil. model:			.997	1.751	2.315	5.063

Experimental Pressure Drop			
Axial Coordinate feet	psi	P _i - P _{i-1} chart divisions	Total ΔP psi
1			
2	-.750	9.5	-.750
3	-.757	10.5	-1.507
4	-.760	11.0	-2.267
5	-.833	19.0	-3.100
6	-.884	28.0	-3.984
7	-.920	33.0	-4.904
8	-.869	26.0	-5.773
9	-.746	9.0	-6.519

	Equilibrium Model	Non-Equilibrium Model
Axial position of net vapor formation:	5.59 ft.	4.30 ft.
Exit mass quality:	.1183	.1193
Two-phase pressure drop:	-2.895 psi	-3.998 psi

Table 13. Results of Predictive Methods and Experimental Data

System pressure = 175 psia Inlet temperature = 266°F
 Mass flux = 1987725 lb_m/hr-ft² Inlet Reynolds number = 115606
 Heat flux (wall) = 28387 Btu/hr-ft² Room temperature = 73°F

Predictive Methods						
Model	Viscosity x 10 ³ lb _m /ft-sec		ΔP _a psi	ΔP _g psi	ΔP _f psi	Total ΔP psi
Homogeneous	.1370	(1)	1.766	1.133	1.709	4.608
	.1574	(2)			1.740	4.639
	.1829	(3)			1.773	4.672
	.2555	(4)			1.853	4.752
Martinelli-Nelson			1.446	1.150	3.049	5.644
Baroczy			1.446	1.150	2.725	5.321
Armand-Lottes-Levy						
Equilibrium model:			1.222	1.259	2.633	5.115
Non-equil. model:			1.226	1.834	3.066	6.128

Experimental Pressure Drop				
Axial Coordinate feet	psi	P _i - P _{i-1} chart divisions	Total ΔP psi	
1				
2	-.753	10.0		-.753
3	-.757	10.5		-1.510
4	-.789	15.0		-2.299
5	-.855	24.0		-3.154
6	-.905	31.0		-4.059
7	-.920	33.0		-4.979
8	-.818	19.0		-5.797
9	-.789	5.0		-6.586
			Equilibrium Model	Non-Equilibrium Model
Axial position of net vapor formation:	5.04 ft.			3.76 ft.
Exit mass quality:	.1523			.1530
Two-phase pressure drop:	-3.394 psi			-4.482 psi

Table 14. Results of Predictive Methods and Experimental Data

System pressure = 175 psia Inlet temperature = 266°F
 Mass flux = 1987725 lb_m/hr-ft² Inlet Reynolds number = 115606
 Heat flux (wall) = 31320 Btu/hr-ft² Room temperature = 73°F

Predictive Methods						
Model	Viscosity x 10 ³ lb _m /ft-sec		ΔP _a psi	ΔP _g psi	ΔP _f psi	Total ΔP psi
Homogeneous	.1370	(1)	2.181	1.163	2.140	5.483
	.1631	(2)			2.187	5.531
	.1958	(3)			2.240	5.583
	.2833	(4)			2.353	5.696
Martinelli-Nelson			1.733	1.200	3.878	6.811
Baroczy			1.733	1.200	3.504	6.437
Armand-Lottes-Levy Equilibrium model:			1.447	1.316	3.445	6.209
Non-equil. model:			1.450	1.884	3.897	7.231

Experimental Pressure Drop				
Axial Coordinate feet	psi	P _i - P _{i-1} chart divisions		Total ΔP psi
1				
2	-.753	10.0		-.753
3	-.768	12.0		-1.521
4	-.840	22.0		-2.361
5	-.884	28.0		-3.245
6	-.913	32.0		-4.158
7	-.876	27.0		-5.034
8	-.905	31.0		-5.939
9	-.833	21.0		-6.772
			Equilibrium Model	Non-Equilibrium Model
Axial position of net vapor formation:	4.57 ft.			3.28 ft.
Exit mass quality:	.1881			.1886
Two-phase pressure drop:	-3.907 psi			-5.014 psi

Table 15. Results of Predictive Methods
and Experimental Data

System pressure = 175 psia Inlet temperature = 266°F
 Mass flux = 1987725 lb_m/hr-ft² Inlet Reynolds number = 115606
 Heat flux (wall) = 20762 Btu/hr-ft² Room temperature = 77°F

Predictive Methods					
Model	Viscosity x 10 ³ lb _m /ft-sec	ΔP _a psi	ΔP _g psi	ΔP _f psi	Total ΔP psi
Homogeneous		(1)			
		(2)			
		(3)			
		(4)			
Martinelli-Nelson					
Baroczy					
Armand-Lottes-Levy					
Equilibrium model:					
Non-equil. model:					

Experimental Pressure Drop				
Axial Coordinate		P _i - P _{i-1}		Total ΔP
feet	psi	chart divisions		psi
1				
2	-.736	8.0		-.736
3	-.747	9.5		-1.483
4	-.747	9.5		-2.230
5	-.762	11.5		-2.992
6	-.805	17.5		-3.797
7	-.903	21.0		-4.700
8	-.907	31.5		-5.607
9	-.845	23.0		-6.452
		Equilibrium Model	Non-Equilibrium Model	
Axial position of net vapor formation:	6.90 ft.		5.61 ft.	
Exit mass quality:	.0592		.0617	
Two-phase pressure drop:	-1.846 psi		-2.972 psi	

Table 16. Results of Predictive Methods and Experimental Data

System pressure = 175 psia Inlet temperature = 266°F
 Mass flux = 1987725 lb_m/hr-ft² Inlet Reynolds number = 115606
 Heat flux (wall) = 23281 Btu/hr-ft² Room temperature = 77°F

Predictive Methods					
Model	Viscosity x 10 ³ lb _m /ft-sec	ΔP _a psi	ΔP _g psi	ΔP _f psi	Total ΔP psi
Homogeneous		(1)			
		(2)			
		(3)			
		(4)			
Martinelli-Nelson					
Baroczy					
Armand-Lottes-Levy					
Equilibrium model:					
Non-equil. model:					

Experimental Pressure Drop			
Axial Coordinate feet	psi	P _i - P _{i-1} chart divisions	Total ΔP psi
1			
2	-.740	8.5	-.740
3	-.747	9.5	-1.487
4	-.758	11.0	-2.245
5	-.773	13.0	-3.018
6	-.845	23.0	-3.863
7	-.925	34.0	-4.788
8	-.896	30.0	-5.684
9	-.816	19.0	-6.500

	Equilibrium Model	Non-Equilibrium Model
Axial position of net vapor formation:	6.15 ft.	4.86 ft.
Exit mass quality:	.0900	.0915
Two-phase pressure drop:	-2.499 psi	-3.590 psi

Table 17. Results of Predictive Methods and Experimental Data

System pressure = 175 psia Inlet temperature = 266°F
 Mass flux = 1987725 lb_m/hr-ft² Inlet Reynolds number = 115606
 Heat flux (wall) = 25598 Btu/hr-ft² Room temperature = 77°F

Predictive Methods					
Model	Viscosity x 10 ³ lb _m /ft-sec	ΔP _a psi	ΔP _g psi	ΔP _f psi	Total ΔP psi
Homogeneous		(1)			
		(2)			
		(3)			
		(4)			
Martinelli-Nelson					
Baroczy					
Armand-Lottes-Levy					
Equilibrium model:					
Non-equil. model:					

Experimental Pressure Drop			
Axial Coordinate feet	psi	P _i - P _{i-1} chart divisions	Total ΔP psi
1			
2	-.740	8.5	-.740
3	-.747	9.5	-1.487
4	-.769	12.5	-2.256
5	-.823	20.0	-3.079
6	-.874	27.0	-3.953
7	-.918	33.0	-4.871
8	-.845	23.0	-5.716
9	-.780	14.0	-6.496
		Equilibrium Model	Non-Equilibrium Model
Axial position of net vapor formation:	5.59 ft.		4.30 ft.
Exit mass quality:	.1183		.1193
Two-phase pressure drop:	-2.899 psi		-3.990 psi

Table 18. Results of Predictive Methods
and Experimental Data

System pressure = 175 psia Inlet temperature = 266°F
 Mass flux = 1987725 lb_m/hr-ft² Inlet Reynolds number = 115606
 Heat flux (wall) = 28387 Btu/hr-ft² Room temperature = 77°F

Predictive Methods					
Model	Viscosity x 10 ³ lb _m /ft-sec	ΔP_a psi	ΔP_g psi	ΔP_f psi	Total ΔP psi
Homogeneous	(1)				
	(2)				
	(3)				
	(4)				

Martinelli-Nelson

Baroczy

Armand-Lottes-Levy

Equilibrium model:

Non-equil. model:

Experimental Pressure Drop			
Axial Coordinate feet	psi	$P_i - P_{i-1}$ chart divisions	Total ΔP psi
1			
2	-.744	9.0	-.744
3	-.755	10.5	-1.499
4	-.802	17.0	-2.301
5	-.852	24.0	-3.153
6	-.889	29.0	-4.042
7	-.896	30.0	-4.938
8	-.845	23.0	-5.783
9	-.820	19.5	-6.603

	Equilibrium Model	Non-Equilibrium Model
Axial position of net vapor formation:	5.04 ft.	3.76 ft.
Exit mass quality:	.1523	.1530
Two-phase pressure drop:	-3.411 psi	-4.499 psi

Table 19. Results of Predictive Methods and Experimental Data

System pressure = 175 psia Inlet temperature = 266°F
 Mass flux = 1987725 lb_m/hr-ft² Inlet Reynolds number = 115606
 Heat flux (wall) = 31320 Btu/hr-ft² Room temperature = 77°F

Predictive Methods					
Model	Viscosity x 10 ³ lb _m /ft-sec	ΔP_a psi	ΔP_g psi	ΔP_f psi	Total ΔP psi
Homogeneous	(1)				
	(2)				
	(3)				
	(4)				

Martinelli-Nelson

Baroczy

Armand-Lottes-Levy

Equilibrium model:

Non-equil. model:

Experimental Pressure Drop			
Axial Coordinate feet	psi	$P_i - P_{i-1}$ chart divisions	Total ΔP psi
1			
2	-.751	10.0	-.751
3	-.765	12.0	-1.516
4	-.820	19.5	-2.336
5	-.881	28.0	-3.217
6	-.911	32.0	-4.128
7	-.881	28.0	-5.009
8	-.889	29.0	-5.898
9	-.860	25.0	-6.758

	Equilibrium Model	Non-Equilibrium Model
Axial position of net vapor formation:	4.57 ft.	3.28 ft.
Exit mass quality:	.1881	.1886
Two-phase pressure drop:	-3.919 psi	-5.010 psi

Table 20. Results of Predictive Methods and Experimental Data

System pressure = 195 psia Inlet temperature = 262°F
 Mass flux = 1051602 lb_m/hr-ft² Inlet Reynolds number = 60220
 Heat flux (wall) = 13873 Btu/hr-ft² Room temperature = 78°F

Predictive Methods						
Model	Viscosity x 10 ³ lb _m /ft-sec		ΔP _a psi	ΔP _g psi	ΔP _f psi	Total ΔP psi
Homogeneous	.1295	(1)	.093	.381	.073	.548
	.1332	(2)			.074	.549
	.1381	(3)			.074	.549
	.1556	(4)			.075	.550
Martinelli-Nelson			.174	.375	.108	.657
Baroczy			.174	.375	.107	.656
Armand-Lottes-Levy Equilibrium model:			.073	.393	.084	.550
Non-equil. model:			.092	.985	.200	1.277

Experimental Pressure Drop			
Axial Coordinate feet	psi	P _i - P _{i-1} chart divisions	Total ΔP psi
1			
2	-.642	-5.0	-.642
3	-.642	-5.0	-1.284
4	-.634	-6.0	-1.918
5	-.645	-4.5	-2.563
6	-.656	-3.0	-3.219
7	-.652	-3.5	-3.871
8	-.642	-5.0	-4.513
9	-.598	-11.0	-5.111
	Equilibrium Model	Non-Equilibrium Model	
Axial position of net vapor formation:	8.126 ft.	6.838 ft.	
Exit mass quality:	.0325	.0411	
Two-phase pressure drop:	-.523 psi	-1.346 psi	

Table 21. Results of Predictive Methods and Experimental Data

System pressure = 195 psia Inlet temperature = 262°F
 Mass flux = 1051602 lb_m/hr-ft² Inlet Reynolds number = 60220
 Heat flux (wall) = 15945 Btu/hr-ft² Room temperature = 78°F

Model	Predictive Methods				
	Viscosity x 10 ³ lb _m /ft-sec	ΔP_a psi	ΔP_g psi	ΔP_f psi	Total ΔP psi
Homogeneous	.1295 (1)	.237	.697	.202	1.136
	.1394 (2)			.204	1.138
	.1524 (3)			.206	1.140
	.1957 (4)			.213	1.147
Martinelli-Nelson		.226	.688	.335	1.249
Baroczy		.226	.688	.347	1.261
Armand-Lottes-Levy Equilibrium model:		.176	.744	.257	1.177
Non-equil. model:		.184	1.317	.390	1.890

Experimental Pressure Drop			
Axial Coordinate feet	psi	$P_i - P_{i-1}$ chart divisions	Total ΔP psi
1			
2	-.642	-5.0	-.642
3	-.638	-5.5	-1.280
4	-.634	-6.0	-1.914
5	-.642	-5.0	-2.556
6	-.649	-4.0	-3.205
7	-.649	-4.0	-3.854
8	-.623	-7.5	-4.477
9	-.562	-16.0	-5.039
	Equilibrium Model	Non-Equilibrium Model	
Axial position of net vapor formation:	7.070 ft.	5.782 ft.	
Exit mass quality:	.0826	.0867	
Two-phase pressure drop:	-1.141 psi	-1.976 psi	

Table 22. Results of Predictive Methods and Experimental Data

System pressure = 195 psia Inlet temperature = 252°F
 Mass flux = 1188084 lb_m/hr-ft² Inlet Reynolds number = 65264
 Heat flux (wall) = 18274 Btu/hr-ft² Room temperature = 80°F

Predictive Methods						
Model	Viscosity x 10 ³ lb _m /ft-sec	ΔP_a psi	ΔP_g psi	ΔP_f psi	Total ΔP psi	
Homogeneous	.1295 (1)	.089	.254	.056	.399	
	.1323 (2)			.056	.399	
	.1359 (3)			.056	.399	
	.1490 (4)			.057	.400	
Martinelli-Nelson		.111	.250	.079	.440	
Baroczy		.111	.250	.077	.438	
Armand-Lottes-Levy Equilibrium model:		.071	.260	.061	.392	
Non-equil. model:		.107	.852	.206	1.165	

Experimental Pressure Drop				
Axial Coordinate feet	psi	$P_i - P_{i-1}$ chart divisions	Total ΔP psi	
1				
2	-.659	-2.5	-.659	
3	-.662	-2.0	-1.321	
4	-.659	-2.5	-1.980	
5	-.669	-1.0	-2.649	
6	-.688	1.5	-3.337	
7	-.680	.5	-4.017	
8	-.706	4.0	-4.723	
9	-.626	-7.0	-5.349	

	Equilibrium Model	Non-Equilibrium Model
Axial position of net vapor formation:	8.440 ft.	7.151 ft.
Exit mass quality:	.0243	.0372
Two-phase pressure drop:	-.351 psi	-1.225 psi

Table 23. Results of Predictive Methods and Experimental Data

System pressure = 195 psia Inlet temperature = 248°F
 Mass flux = 1194089 lb_m/hr-ft² Inlet Reynolds number = 64603
 Heat flux (wall) = 20214 Btu/hr-ft² Room temperature = 80°F

Model	Predictive Methods				
	Viscosity x 10 ³ lb _m /ft-sec	ΔP_a psi	ΔP_g psi	ΔP_f psi	Total ΔP psi
Homogeneous	.1295 (1)	.148	.354	.091	.593
	.1341 (2)			.092	.593
	.1401 (3)			.092	.594
	.1616 (4)			.094	.596
Martinelli-Nelson		.173	.347	.138	.658
Baroczy		.173	.347	.134	.654
Armand-Lottes-Levy Equilibrium model:		.116	.366	.103	.586
Non-equil. model:		.147	.945	.261	1.353

Experimental Pressure Drop			
Axial Coordinate feet	psi	$P_i - P_{i-1}$ chart divisions	Total ΔP psi
1			
2	-.666	-1.5	-.666
3	-.662	-.20	-1.328
4	-.662	-2.0	-1.990
5	-.673	-0.5	-2.663
6	-.684	1.0	-3.347
7	-.698	3.0	-4.045
8	-.709	4.5	-4.754
9	-.637	-5.5	-5.391

	Equilibrium Model	Non-Equilibrium Model
Axial position of net vapor formation:	8.163 ft.	6.874 ft.
Exit mass quality:	.0400	.0512
Two-phase pressure drop:	-.533 psi	-1.434 psi

Table 24. Results of Predictive Methods and Experimental Data

System pressure = 195 psia Inlet temperature = 238°F
 Mass flux = 1208972 lb_m/hr-ft² Inlet Reynolds number = 62675
 Heat flux (wall) = 22701 Btu/hr-ft² Room temperature = 80°F

Predictive Methods						
Model	Viscosity x 10 ³ lb _m /ft-sec		ΔP _a psi	ΔP _g psi	ΔP _f psi	Total ΔP psi
Homogeneous	.1295	(1)	.079	.181	.040	.299
	.1319	(2)			.040	.299
	.1349	(3)			.040	.299
	.1461	(4)			.040	.300
Martinelli-Nelson			.099	.179	.056	.334
Baroczy			.099	.179	.054	.332
Armand-Lottes-Levy Equilibrium model:			.063	.184	.045	.292
Non-equil. model:			.115	.772	.195	1.082

Experimental Pressure Drop			
Axial Coordinate feet	psi	P _i - P _{i-1} chart divisions	Total ΔP psi
1			
2	-.662	-2.0	-.662
3	-.669	-1.0	-1.361
4	-.666	-1.5	-2.027
5	-.677	0	-2.704
6	-.688	1.5	-3.392
7	-.706	4.0	-4.098
8	-.713	5.0	-4.801
9	-.662	-2.0	-5.463

	Equilibrium Model	Non-Equilibrium Model
Axial position of net vapor formation:	8.608 ft.	7.320 ft.
Exit mass quality:	.0208	.0386
Two-phase pressure drop:	-.259 psi	-1.147 psi

Table 25. Results of Predictive Methods and Experimental Data

System pressure = 195 psia Inlet temperature = 247°F
 Mass flux = 1195585 lb_m/hr-ft² Inlet Reynolds number = 64310
 Heat flux (wall) = 20214 Btu/hr-ft² Room temperature = 80°F

Predictive Methods						
Model	Viscosity x 10 ³ lb _m /ft-sec		ΔP _a psi	ΔP _g psi	ΔP _f psi	Total ΔP psi
Homogeneous	.1295	(1)	.120	.296	.071	.488
	.1332	(2)			.072	.488
	.1380	(3)			.072	.488
	.1554	(4)			.073	.489
Martinelli-Nelson			.145	.291	.105	.541
Baroczy			.145	.291	.102	.538
Armand-Lottes-Levy Equilibrium model:			.095	.305	.079	.479
Non-equil. model:			.131	.888	.233	1.252

Experimental Pressure Drop			
Axial Coordinate feet	psi	P _i - P _{i-1} chart divisions	Total ΔP psi
1			
2	-.659	-2.5	-.659
3	-.673	-0.5	-1.332
4	-.662	-2.0	-1.994
5	-.669	-1.0	-2.663
6	-.684	1.0	-3.347
7	-.691	2.0	-4.038
8	-.717	5.5	-4.755
9	-.637	-5.5	-5.392

	Equilibrium Model	Non-Equilibrium Model
Axial position of net vapor formation:	8.322 ft.	7.033 ft.
Exit mass quality:	.0324	.0451
Two-phase pressure drop:	-.432 psi	-1.330 psi

Table 26. Results of Predictive Methods and Experimental Data

System pressure = 195 psia Inlet temperature = 228°F
 Mass flux = 606912 lb_m/hr-ft² Inlet Reynolds number = 30121
 Heat flux (wall) = 15945 Btu/hr-ft² Room temperature = 77°F

Predictive Methods						
Model	Viscosity x 10 ³ lb _m /ft-sec		ΔP_a psi	ΔP_g psi	ΔP_f psi	Total ΔP psi
Homogeneous	.1295	(1)	.145	.609	.104	.858
	.1490	(2)			.106	.860
	.1748	(3)			.108	.862
	.2514	(4)			.114	.868
Martinelli-Nelson			.122	.620	.185	.927
Baroczy			.122	.620	.245	.987
Armand-Lottes-Levy Equilibrium model:			.096	.687	.143	.926
Non-equil. model:			.099	1.227	.204	1.531

Experimental Pressure Drop			
Axial Coordinate feet	psi	$P_i - P_{i-1}$ chart divisions	Total ΔP psi
1			
2	-.631	-6.5	-.631
3	-.639	-5.5	-1.270
4	-.631	-6.5	-1.901
5	-.631	-6.5	-2.532
6	-.620	-8.0	-3.152
7	-.595	-11.5	-3.747
8	-.562	-16.0	-4.309
9	-.533	-20.0	-4.842

	Equilibrium Model	Non-Equilibrium Model
Axial position of net vapor formation:	6.950 ft.	5.661 ft.
Exit mass quality:	.1521	.1581
Two-phase pressure drop:	-1.126 psi	-1.901 psi

Table 27. Results of Predictive Methods and Experimental Data

System pressure = 195 psia Inlet temperature = 228°F
 Mass flux = 606912 lb_m/hr-ft² Inlet Reynolds number = 30121
 Heat flux (wall) = 17872 Btu/hr-ft² Room temperature = 77°F

Predictive Methods						
Model	Viscosity x 10 ³ lb _m /ft-sec		ΔP _a psi	ΔP _g psi	ΔP _f psi	Total ΔP psi
Homogeneous	.1295	(1)	.223	.699	.178	1.099
	.1620	(2)			.183	1.104
	.2050	(3)			.188	1.110
	.3161	(4)			.200	1.121
Martinelli-Nelson			.177	.738	.318	1.233
Baroczy			.177	.738	.454	1.369
Armand-Lottes-Levy Equilibrium model:			.135	.821	.261	1.219
Non-equil. model:			.137	1.352	.327	1.817

Experimental Pressure Drop			
Axial Coordinate feet	psi	P _i - P _{i-1} chart divisions	Total ΔP psi
1			
2	-.639	-5.5	-.639
3	-.635	-6.0	-1.274
4	-.635	-6.0	-1.909
5	-.624	-7.5	-2.533
6	-.602	-10.5	-3.135
7	-.584	-13.0	-3.719
8	-.551	-17.5	-4.270
9	-.544	-18.5	-4.814

	Equilibrium Model	Non-Equilibrium Model
Axial position of net vapor formation:	6.200 ft.	4.911 ft.
Exit mass quality:	.2328	.2362
Two-phase pressure drop:	-1.563 psi	-2.337 psi

Table 28. Results of Predictive Methods and Experimental Data

System pressure = 195 psia Inlet temperature = 228°F
 Mass flux = 606912 lb_m/hr-ft² Inlet Reynolds number = 30121
 Heat flux (wall) = 20214 Btu/hr-ft² Room temperature = 77°F

Predictive Methods						
Model	Viscosity x 10 ³ lb _m /ft-sec		ΔP _a psi	ΔP _g psi	ΔP _f psi	Total ΔP psi
Homogeneous	.1295	(1)	.316	.745	.277	1.338
	.1811	(2)			.289	1.350
	.2487	(3)			.302	1.363
	.3946	(4)			.321	1.383
Martinelli-Nelson			.243	.812	.486	1.541
Baroczy			.243	.812	.731	1.786
Armand-Lottes-Levy Equilibrium model:			.177	.912	.415	1.506
Non-equil. model:			.177	1.433	.488	2.099

Experimental Pressure Drop				
Axial Coordinate feet	psi	P _i - P _{i-1} chart divisions	Total ΔP psi	
1				
2	-.642	-5.0		-.642
3	-.631	-6.5		-1.273
4	-.631	-6.5		-1.904
5	-.620	-8.0		-2.524
6	-.591	-12.0		-3.115
7	-.570	-15.0		-3.685
8	-.548	-18.0		-4.233
9	-.533	-20.0		-4.766
			Equilibrium Model	Non-Equilibrium Model
Axial position of net vapor formation:			5.482 ft.	4.193 ft.
Exit mass quality:			.3308	.3327
Two-phase pressure drop:			-1.957 psi	-2.743 psi

BIBLIOGRAPHY

1. Ahmad, S. Y., "Axial Distribution of Bulk Temperature and Void Fraction in a Heated Channel with Inlet Subcooling," Journal of Heat Transfer, ASME Transaction, Series C, Volume 92, 1970, p. 595.
2. Baroczy, C. J., "A Systematic Correlation for Two-Phase Pressure Drop," A.I.Ch.E. Reprint No. 37, paper presented at the Eighth National Heat Transfer Conference, Los Angeles, August, 1965.
3. Bijwaard, G., Staub, F. W., and Zuber, N., "A Program of Two-Phase Flow Investigation," Eleventh Quarterly Report, October-December, 1965, General Electric Co., San Jose, California, Report No. GEAP 5067, Euratom Report No. EURAEC 1575.
4. Collier, J. G., Convective Boiling and Condensation, McGraw-Hill Book Company (UK) Limited, 1972.
5. Cicchitti, A., Lombardi, C., Silvestri, M., Soldaini, G., and Zavattarelli, "Two-Phase Cooling Experiments-- Pressure Drop, Heat Transfer, and Burnout Measurements," Energia Nucleare, 7(6), 1960, pp. 407-425.
6. Davidson, W. F. et al., "Studies of Heat Transmission Through Boiler Tubing at Pressures from 500 to 3300 Pounds," Trans. ASME, 65, 1943, pp. 553-591.
7. Hagendorn, A. R. and Brown, K. E., "Experimental Study of Pressure Gradients Occurring During Continuous Two-Phase Flow in Small Diameter Vertical Conduits," Transactions ASME, 17, April, 1965, pp. 136-147.
8. Isbin, H. S., May, J. E., and DaCruz, A. J. R., "Two-Phase Steam-Water Critical Flow," The American Institute of Chemical Engineering Journal, 3, 1957, p. 361.
9. Isbin, H. S. et al., "Two-Phase Steam-Water Pressure Drops," Nuclear Engineering Part VI, Chem. Eng. Symp. Series No. 23, 55, 1959, pp. 75-84.
10. Ishii, M., "Thermally Induced Flow Instabilities in Two-Phase Mixtures in Thermal Equilibrium," Ph.D. Thesis, Georgia Institute of Technology, June, 1971.

11. Kocamustafaogullari, G., "Thermo-Fluid Dynamics of Separated Two-Phase Flow," Ph.D. Thesis, Georgia Institute of Technology, December, 1971.
12. Kroeger, P. G. and Zuber, N., "An Analysis of the Effects of Various Parameters on the Average Void Fractions in Subcooled Boiling," International Journal of Heat and Mass Transfer, 11, 1968, p. 211.
13. Levy, S., "Forced Convection Subcooled Boiling-- Prediction of Vapor Volumetric Fraction," International Journal of Heat and Mass Transfer, 10, 1967, p. 591.
14. Lockhart, R. W. and Martinelli, R. C., "Proposed Correlation of Data for Isothermal Two-Phase Two-Component Flow in Pipes," Chem. Eng. Prog., 45, 1945, p. 39.
15. Martinelli, R. C. and Nelson, D. B., "Prediction of Pressure Drop During Forced-Circulation Boiling of Water," Transactions ASME, 70, 1948, p. 695.
16. McAdams, W. H., Woods, W. K., and Heroma, C. C., "Vaporization Inside Horizontal Tubes--II--Benzene-Oil Mixtures," Transactions ASME, 64, 1942, p. 193.
17. Owens, W. L., "Two-Phase Pressure Gradient," International Developments in Heat Transfer, Part II, ASME, 1961, pp. 363-368.
18. Saha, P., "Thermally Induced Two-Phase Flow Instabilities, Including the Effect of Thermal Non-Equilibrium Between the Phases," Ph.D. Thesis, Georgia Institute of Technology, June, 1974.
19. Saha, P. and Zuber, N., "Point of Net Vapor Generation and Vapor Void Fraction in Subcooled Boiling," paper to be presented to the Fifth International Heat Transfer Conference, Tokyo, Japan, September, 1974.
20. Tong, L. S., Boiling Heat Transfer and Two-Phase Flow, John Wiley and Sons, Inc., 1965.
21. Wallis, G. B., One-Dimensional Two-Phase Flow, McGraw-Hill Book Company, 1969.
22. Zuber, N. and Dougherty, D. E., "Liquid Metals Challenge to the Traditional Methods of Two-Phase Flow Investigations," Symposium on Two-Phase Flow Dynamics, Eindhoven, Vol. 1, p. 1091, September, 1967.

23. Zuber, N., Staub, F. W., and Bijwaard, G., "Vapor Void Fraction in Subcooled Boiling and Saturated Boiling Systems," Proceedings of the Third International Heat Transfer Conference, 5, A.I.Ch.E., New York, 1966, p.24.
24. Zuber, N., "Flow Excursions and Oscillations in Boiling Two-Phase Flow Systems with Heat Addition," Symposium on Two-Phase Flow Dynamics, Eindhoven, Volume I, September, 1967, p. 1071.
25. Surface Tension of the "Freon" Compounds, Technical Bulletin D-27, E. I. dePont de Nemours and Co., Wilmington, Delaware.
26. Thermodynamic Properties of "Freon" 113, Technical Bulletin T-113A, E. I. dePont de Nemours and Co., Wilmington, Delaware.
27. Transport Properties of "Freon" Fluorocarbons, Technical Bulletin C-30, E. I. duPont de Nemours and Co., Wilmington, Delaware.
28. Martin, R., "Measurement of the Local Void Fraction at High Pressure in a Heating Channel," Nuclear Science and Engineering, Volume 48, 1972, p. 125.
29. Lobachev, A. G., Kolchugin, B. A., Zakharov, E. A. and Kruglikhina, G. G., "Investigation of Vapor Void Fraction in Heated Pipes in Two-Phase Upward and Downward Flow," Teploenergetika, Number 5, 1973, p. 75.
30. Staub, F. W., Walnut, G. E. and Niemi, R. O., "Heat Transfer and Hydraulics--The Effect of Subcooled Voids," Final Report No. NYO - 3679-8. Also, EURAEC-2120, February, 1967-June, 1969.